



Norwegian University  
of Life Sciences

**Master's Thesis 2019 30 ECTS**  
Faculty of Science and Technology

# **Light and Elevated Temperature Induced Degradation in Multicrystalline Silicon Wafers Studied by Hyperspectral Photoluminescence Imaging**

Jon-Fredrik Blakstad Cappelen  
Environmental Physics and Renewable Energy



## PREFACE

---

This thesis will complete my master's degree in technology at the Norwegian University of Life Sciences (NMBU). I will take this opportunity to thank my supervisors Ingunn Burud and Espen Olsen for helpful advice and guidance through the endeavour of writing this thesis. Next, I will thank my lab partner Torbjørn Mehl for good cooperation and conversation through long sessions at the lab. Furthermore, I will thank the PV research group at REALTEK (NMBU) for great discussions and nice Monday meetings. Too, I will thank the LETuP project, especially Rune Søndena at IFE for providing wafer samples to study. Lastly, I thank my wonderful fiancée Karoline for steady direction and comforting embraces through a long, last semester.



## ABSTRACT

---

Light and elevated temperature induced degradation (LeTID) has become a profound problem for the new PERC cells, reducing performance by as much as 16% during operation. The mechanism that governs the degradation is not fully understood, but some effect caused by hydrogen in the bulk of the cell is one of the suggested causes. High performance multicrystalline silicon (hpmc-Si) p-type wafers of different processing are investigated for LeTID using a hyperspectral photoluminescence (HSPL) imaging setup. As cut, phosphorus diffusion gettered (PDG) and gettered hydrogen bulk passivated wafer samples, with and without surface passivation, were processed with light soaking and elevated temperatures, with imaging at 90 K at intervals of the processing. LeTID was only observed in the samples with both surface passivation, PDG and hydrogen bulk passivation. This supports the hypothesis that bulk hydrogen is involved with the LeTID mechanism and suggests that a high charge carrier density is required. Defect related luminescence (DRL), PL signals correlated with defects and impurities, did not appear or disappear as a result of LeTID but got reduced intensity as the band-to-band (BB) signal, a PL signal correlated with cell performance, degraded. Both BB and DRL recovered with long time exposure to light and elevated temperature.

## SAMMENDRAG

---

Lys- og økt temperaturforårsaket degradering (LeTID) har vist seg å være et betydelig problem for de nye PERC-solcellene; ytelsen kan reduseres med så mye som 16% mens cellen er i bruk. Mekanismen som står bak denne degraderingen er ikke forstått fullt ut, men en effekt som skyldes hydrogen inne i cellen er en foreslått årsak. High performance multikrystallinsk silisium (hpmc-Si) p-type wafere med forskjellig prosessering har blitt undersøkt for LeTID med et hyperspektralt fotoluminescens (HSPL) avbildningssystem. As cut (nesten ubehandlede), fosfordiffusjon-rensede (PDG) og rensede bulkpassiverte waferprøver, med og uten overflatepassivering, ble behandlet med lys og økt temperatur. De ble avbildet ved 90 kelvin ved varierende intervaller under behandlingen. LeTID ble bare observert i prøvene med både overflatepassivering, PDG-behandling og bulk-hydrogen-passivering. Dette støtter opp under hypotesen om at bulk-hydrogen, hydrogen inne i waferen, er involvert i LeTID mekanismen. Høy ladningsbærertetthet ser også ut til være nødvendig for LeTID-mekanismen. Defektrelatert luminescens (DRL), fotoluminescenssignaler fra defekter og urenheter, verken forsvant eller oppstod med LeTID. DRL-signalene tok derimot og endret intensitet i takt med bånd-til-bånd-signalet (BB), signalet som indikerer wafer med god ytelse, når det ble svekket. Både BB og DRL signalet regenererte med lang eksponering for lys og økt temperatur.

# CONTENTS

---

Preface .....	I
Abstract .....	III
Sammendrag .....	III
Contents .....	IV
List of Abbreviations .....	VII
1 Introduction .....	1
2 Theory .....	3
2.1 Intrinsic Semiconductor .....	3
2.1.1 Direct and Indirect Bandgap .....	4
2.2 Extrinsic Semiconductor .....	5
2.3 The p-n Junction .....	6
2.4 Charge Carrier Pair Generation and Recombination .....	7
2.4.1 Recombination mechanisms .....	7
2.4.2 Lifetime .....	8
2.5 Multicrystalline Wafer Production and Processing .....	10
2.5.1 Casting .....	10
2.5.2 Gettering .....	10
2.5.3 Passivation .....	11
2.6 Photoluminescence .....	12
2.6.1 Band-to-Band Photoluminescence .....	12
2.6.2 Defect Related Luminescence .....	12
2.6.3 Defect Related Luminescence as a Function of Temperature .....	13
2.7 Light and elevated Temperature Induced Degradation .....	14
3 Experimental .....	15
3.1 Samples .....	15
3.1.1 Pre-Processing .....	16

## Contents

3.1.2	Processing.....	18
3.2	Hyperspectral Photoluminescence Imaging .....	19
3.2.1	Hyperspectral Camera.....	19
3.2.2	Line Laser.....	20
3.2.3	Long Pass Filter .....	20
3.2.4	Sample Holder/Cryogenic Cooler .....	20
3.2.5	Frost and Fog Protection .....	21
3.3	Data processing .....	22
3.3.1	Pre-Processing .....	22
3.3.2	Visualization .....	22
3.3.3	Tools for Spectral Analysis.....	23
4	Results and Discussion .....	25
4.1	Initial Analysis on Non-Surface Passivated Samples.....	25
4.2	Initial Analysis on Surface Passivated Samples .....	35
4.3	Further Analysis on the Surface and Bulk Passivated Samples .....	45
4.4	Multivariate Curve Resolution Analysis.....	51
4.5	Rounding of Discussion.....	53
5	Conclusion .....	55
6	References.....	57
	Appendices.....	59
A)	Python function for reading HSPL images into memory .....	59
B)	Python function for sorting the images by processing time.....	61
C)	Python functions for plotting development in the sample-wide BB signal.....	62
D)	Python functions for plotting development of the different photon energies .....	65
E)	Python functions for plotting development in spatial DRL/BB distribution .....	67





## LIST OF ABBREVIATIONS

---

AC	As cut
ALS	Alternating Least Squares
AM	Air Mass
BB	Band-to-band
BSF	Back Surface Field
DRL	Defect Related Luminescence
D1, D2, D3, D4	DRL signals of known photon energy
HSPL	Hyperspectral Photoluminescence
ICA	Independent Component Analysis
LeTID	Light and elevated Temperature Induced Degradation
LETuP	The LETuP project which does research on LeTID
LID	Light Induced Degradation
mc-Si	Multicrystalline Silicon
mono-Si	Monocrystalline Silicon
NMBU	The Norwegian University of Life Sciences
PCA	Principal Component Analysis
PDG(H)	Phosphorus Diffusion Gettering (+ Hydrogenation)
PERC	Passivated Emitter Rear Contact
PL	Photoluminescence
PV	Photovoltaic
SRH	Shockley Read Hall
SWIR	Short Wavelength Infrared



# 1 INTRODUCTION

---

The world has an ever-increasing demand for energy. Especially since the industrial revolution of the late 1700s this demand has been profound, and it has largely been met by the fossil energy source coal and later also oil and gas. These sources will eventually run out<sup>1</sup> and should be replaced before they do so. Devastating changes to the climate are also associated with the burning of fossil fuels<sup>2,3</sup>. To this end, renewable energy sources must emerge as replacements for the fossil fuels. *Photovoltaic* (PV) solar technology is such an energy source with a great promise. For this technology to be viable it must compete with both other renewable sources, such as hydro power and wind, as well as coal, oil and gas. As production has increased and the industry has matured, the price for PV has dropped drastically. For every doubling in accumulated shipped PV power the price has dropped by 23.2% since 1976 and by 39.8% since 2006<sup>4</sup>. The increasingly competitive price, combined with flexible installation on both utility and consumer scale, marks PV solar as a leading renewable energy source.

Commercially available solar modules have increased in average efficiency from 14.7% in 2010 to 18.4% in 2018<sup>4</sup>. These numbers include p-type mc-Si and mono-Si modules, where mono-Si have a higher efficiency. Research mc-Si cells (not modules) have been made with up to 21.9% efficiency<sup>5</sup>. The difference is to some degree caused by modules inherently having lower efficiency as the module area not only accommodates active cell area but also electrical contacts and mechanical support. However, the difference in efficiency is also caused by research cells being made as close to perfection as possible, while the commercial cells are made in large quantities and cost effectively. The gap can be made smaller with improved production techniques if the exact causes for the performance loss can be identified and understood.

One such cause for reduced field performance, when compared to research, is the *light and elevated temperature induced degradation* (LeTID)<sup>6</sup>. Relatively recently this degradation has been made a concern to the solar industry. As new *PERC* cells (Passivated Emitter Rear Contact) are put into use a decrease in efficiency, relative to the initial efficiency of the cells, is observed. This phenomenon is readily observed, but not fully understood<sup>6</sup>.

*Hyperspectral photoluminescence* (HSPL) imaging is an emerging, fast and non-destructive technique for analysis of various materials. Such a setup has been developed at NMBU for analysis of PV material<sup>7,8</sup>. For this thesis I shall use this setup to investigate how different processing affects LeTID in p-type mc-Si wafers. Wafers samples with and without surface passivation, and with varying degree of gettering and bulk passivation, will be light and elevated temperature treated and imaged for the investigation.

## Introduction

Table 1.1: A questing for this thesis: For which type or types of processing will LeTID be observed in a hpmc-Si p-type wafer?

	Surface Passivation Removed	Surface Passivated
As cut		
PDG		
PDGH		

In this thesis I ask the following questions: For which type or types of processing will LeTID be observed in a hpmc-Si p-type wafer? The cells in Table 1.1 represent the different sample processing combinations that will be investigated. A hydrogen effect is suspected to be the mechanism behind LeTID<sup>9,10</sup>. Insight into this hypothesis is hoped to be obtain through this study.

Does LeTID manifest as new defects or does it affect the already present defects? This will be investigated further by analysis of the samples where LeTID is observed.

## 2 THEORY

The goal of this section is to provide the necessary theoretical background relevant to this thesis. Unless other references are stated, the theory and equations in this section is taken from Smets et al.<sup>11</sup>

### 2.1 INTRINSIC SEMICONDUCTOR

A semiconductor is a material which can have characteristics of both electrical conductors and insulators, depending on the circumstances and treatment. The most common semiconductor, both in terms of solar usage<sup>4</sup> and availability in the Earth's crust, is Silicon (Si). This thesis will thus focus on this metal, in its multicrystalline form (mc-Si).

In pure, *intrinsic*, silicon the atoms are arranged in a regular crystalline fashion so that each atom is covalently connected to four other atoms, with an angle of  $109.5^\circ$  between the bindings. The four electrons that each atom shares with its neighbouring atoms are loosely bonded and will be the electrons that are active in the electronics of solar technology.

An isolated atom has certain energy levels that the electrons can occupy. As more atoms bind together the energy levels will "blur into each other", creating *bands* that the electrons can occupy. At the temperature of absolute zero ( $0\text{ K} = -273,15^\circ\text{C}$ ) all the electrons are "at rest", bonded to the atoms in the covalent band, and the material will not conduct electricity. At temperatures above  $0\text{ K}$  some of the electrons will be excited by the thermal energy, out of the *valence band*, into the *conduction band*. In the conduction band the electrons are free to move, allowing them to conduct electricity, hence the name. As the electrons are excited to the conduction band, they leave behind a vacancy of charge called a "hole". Other electrons in the crystal can move to occupy this hole, creating a new hole associated with the atom the electron left. In this way the hole is said to move through the crystal, making them charge carriers as well as the electrons. These concepts are illustrated in Figure 2.1.

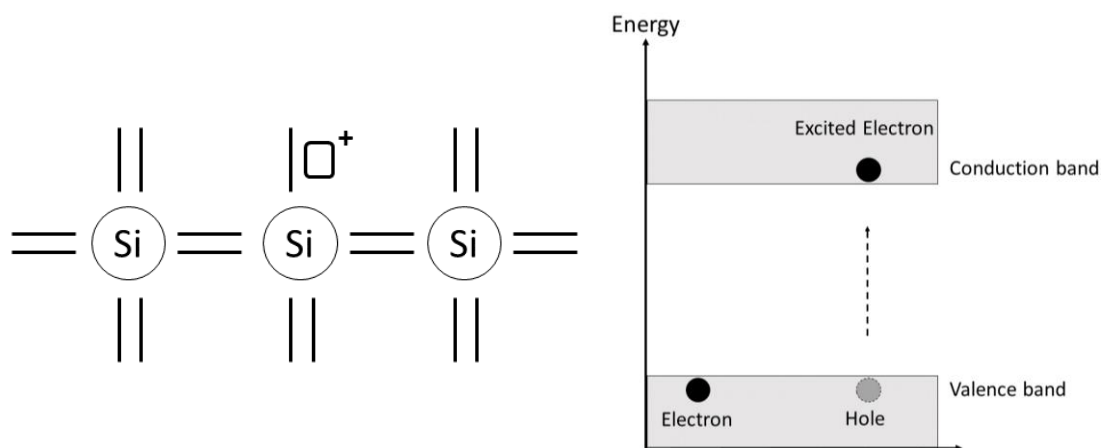


Figure 2.1: Illustration of the structure model for intrinsic silicon and the band model for an intrinsic semiconductor. The middle silicon atom in the structure model is excited, shown by having a positive hole (the square+). The lines are covalent bonds of shared electrons. The band model shows an electron at rest in the valence band, and an excited electron-hole pair with the electron in the conduction band and the hole in the valence band.

## Theory

The difference in energy between the conduction band and the valence band is called the bandgap. The size of the bandgap dictates how well the material will conduct electricity. At room temperature (usually taken to be 300 K in semiconductor physics) a semiconductor's intermediate sized bandgap will allow only a few electrons to be excited, making for a poor conductor but not a complete insulator, hence the term semiconductor. To put these statements into numbers; the density of Si-atoms in intrinsic silicon is approximately  $5 \cdot 10^{22} \text{ cm}^{-3}$ , whereas the number of electron-hole pairs at 300 K is approximately  $1.5 \cdot 10^{10} \text{ cm}^{-3}$ .

### 2.1.1 Direct and Indirect Bandgap

So far, the bandgap has been referred to as a fixed size for the given material as it is a useful simplification. However, the valence band and the conduction band vary as a function of momentum of the electrons. For some semiconductors the top of the valence band aligns with the bottom of the conduction band. These semiconductors are said to have a direct bandgap. In such material more electrons will be excited, as only energy is required to excite them. This energy is typically in the form of thermal energy or radiation; *photons*.

Silicon has an indirect bandgap as the valence band top and the conduction bottom do not align. This leads to fewer excited electrons, as both energy and momentum must simultaneously be transferred to the electrons to excite them. The momentum is transferred to the electrons as *phonons*, which are quantified vibrations in the crystal lattice. The indirect bandgap material is less likely to absorb the solar radiation as both the photons and phonons must interact with the electrons simultaneously. Direct and indirect bandgaps are illustrated in Figure 2.2.

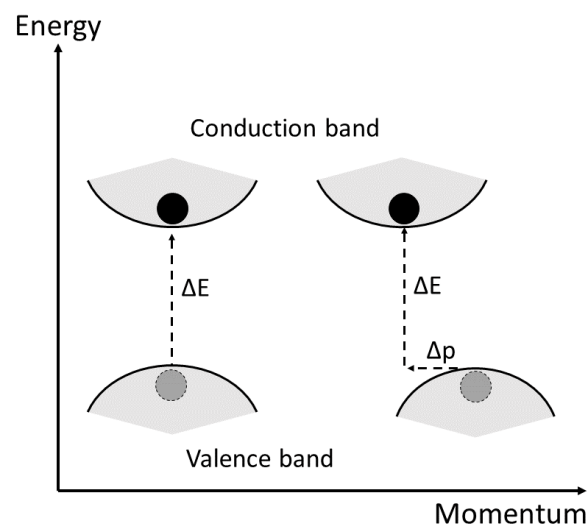


Figure 2.2: Illustration of a direct, on the left, and indirect bandgap, on the right. For the direct bandgap only an energy  $\Delta E$  is needed for excitation. For the indirect bandgap momentum  $\Delta p$  is also needed for excitation.

In practice this means that silicon solar cells, and cells of other indirect bandgap materials, need to be significantly thicker than direct bandgap solar cells. The samples used for this thesis were about 160  $\mu\text{m}$  thick.

## 2.2 EXTRINSIC SEMICONDUCTOR

As stated earlier, intrinsic semiconductors make for poor conductors. The solution to this problem is to add other materials to the pure silicon, a technique called *doping*. The most common type of doping for solar use is p-type doping<sup>4</sup>. The wafers used for this thesis are of the p-type variant. P-doping involves adding a trivalent atom, usually Boron (B)<sup>4</sup>. The boron atom takes the place of a silicon atom in the crystal. The boron is now called an acceptor, as it tends to accept or receive electrons from the neighbouring atoms. This way the boron creates holes in the crystal, and thus adding charge carriers and increasing the conductivity of the semiconductor.

The alternative is n-doping where a pentavalent atom is added to the intrinsic silicon, usually phosphorus (P). The phosphorus will replace a silicon atom and bring an extra, very loosely bonded electron to the structure, potentially adding charge carriers and increasing conductivity. The phosphorus is called a donor atom, as it donates or gives electrons. p-type and n-type doping is illustrated with structure models in Figure 2.3.

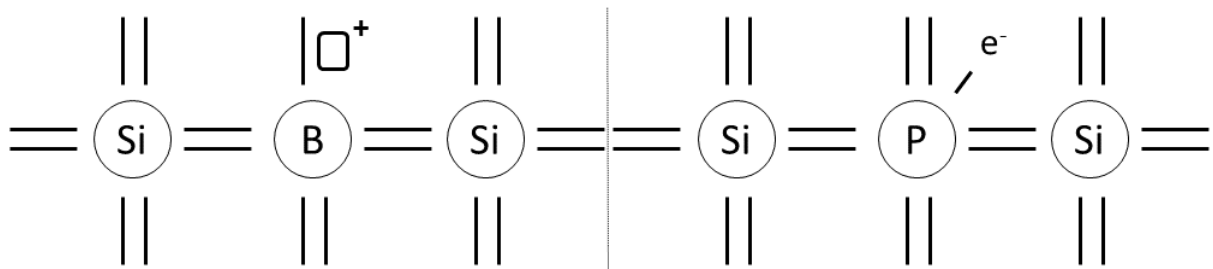


Figure 2.3: Illustration of the structure model for p-doped and n-doped silicon (Si), on the left and right respectively. The Boron (B) in the p-doped silicon is excited and gives a positive hole (square+). The phosphorus (P) in the n-doped silicon has an extra electron ( $e^-$ ) that is easily excited.

Common levels of doping are around  $10^{16} \text{ cm}^{-3}$ . At room temperature (300 K) all the doping atoms will be excited and by far outnumber the  $1.5 \cdot 10^{10} \text{ cm}^{-3}$  intrinsically excited electrons-hole pairs. Electron-hole pairs will be generated and recombine at equal rates for the given temperature and doping, settling at an equilibrium.

## 2.3 THE P-N JUNCTION

The goal of doping is not to increase the electrical conductivity in and of itself, but to allow the semiconducting material to be used to generate an electrical potential and a current. For this to work, the holes and electrons must be separated and conducted to an external circuit before they *recombine*; the excited electrons go to the valence band to fill charge vacancies (more on this in Section 2.4). This is achieved by having a n-doped region next to the p-doped region, a *p-n junction*. The mobile electrons of the n-doped region will diffuse to fill the holes in the p-doped region, creating a region without any free charge carriers: *The depletion zone*. An electrical field will arise, pointing from the n-region to the p-region, as the p-region now contains a net negative charge while the n-region contains a net positive charge. When the electrical field and the concentration gradient is in balance, there will be no net diffusion of electrons across the p-n junction. The p-n junction is illustrated in Figure 2.4.

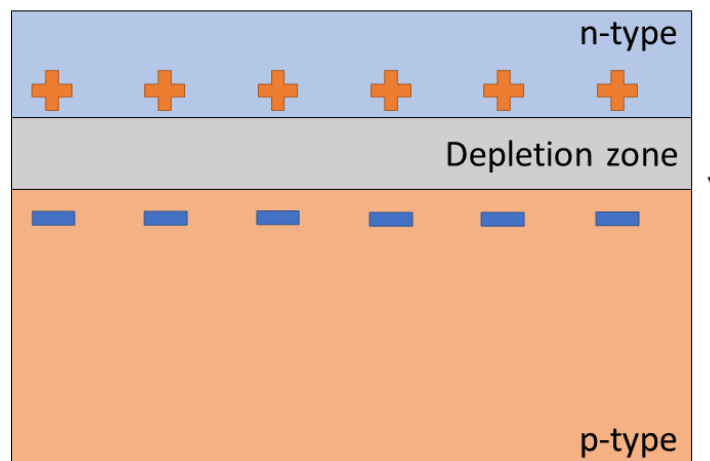


Figure 2.4: Illustration of the p-n junction formed in a p-type semiconductor. It is called a p-type semiconductor as the substrate is p-doped, with only a thin layer of n-doped semiconductor added at the top. The n-type layer is added by diffusing n-dopant into the p-type substrate. A depletion zone forms at the interface between the two layers. The arrow indicates the direction of the internal electrical field. The pluses and minuses represent net positive and negative charges respectively.



## 2.4 CHARGE CARRIER PAIR GENERATION AND RECOMBINATION

For solar use, additional electron-hole pairs are generated when light of sufficient photon energy illuminates the solar cell. These new pairs again create a concentration gradient, driving electrons and holes to cross the p-n junction. Electrons will flow from the p-type region into the n-type region, and holes from n-type to p-type. If no external circuit is connected, this flow will be balanced by a recombination flow which increases as the electrical field of the p-n junction is weakened by the additional flow of electrons and holes into the n- and p-type regions respectively. At this new illumination-equilibrium, with no external circuit, the electrical potential called *open circuit voltage* will stand across the p-type and n-type side of the cell. This voltage can drive a current through an external circuit connecting the n-side and p-side, delivering power for useful work.

The voltage and current of the cell, and thus the power and efficiency, will increase with lower rate of recombination and decrease with higher rate of recombination. Low recombination rates are thus desired for solar use.

### 2.4.1 Recombination mechanisms

This subsection will give an overview of the mechanisms which contribute to recombination.

#### 2.4.1.1 *Direct recombination*

As an electron can be excited to the conduction band by absorbing energy, so can it be relaxed or deexcited directly by releasing energy equal to the bandgap. This process is usually radiative; the energy is released as a single photon. This process is intrinsic to the material; it cannot be lowered to increase efficiency. For silicon however, this process is less of a concern as the indirect bandgap yields a low level of direct recombination.

#### 2.4.1.2 *Shockley-Read-Hall Recombination*

Impurities and lattice defects in the solar material can create energy levels in the otherwise forbidden bandgap. Recombination as electrons are deexcited through these energy levels are called *Shockley-Read-Hall* (SRH) recombination. This form of recombination is of most importance for this thesis, as it is these impurities and lattice defects we wish to detect.

#### 2.4.1.3 *Auger Recombination*

Auger recombination is a three-particle process where the excited electron is deexcited by giving its energy and momentum to another electron in the conduction band, or to another hole in the valence band as it recombines with a second hole. This recombination is strongly dependent on the density of charge carriers (electrons and holes) and is thus of most importance when the doping level is high, and/or the irradiance is very high. This is typically the case for concentrated photovoltaics.

Furthermore, Auger recombination is more important for indirect bandgap materials, as the recombination is not already dominated by direct combination.

#### 2.4.1.4 Surface Recombination

The previously mentioned recombination mechanisms (Sections 2.4.1.1-2.4.1.3) primarily takes place in the bulk of the material. However, the recombination that occur at the surface is important as well as it will have a detrimental effect on the performance of the cell if not dealt with appropriately. Like SRH recombination, energy levels will occur in the bandgap at the surface of the material as the crystal lattice ends. These energy levels are a consequence of so-called *dangling bonds*; as the atoms at the surface have electrons with no other atoms to bond to they form new energy states. These dangling bonds can be filled through a process called *surface passivation* where a layer of suitable material is deposited on the surface of the semiconductor, bonding to the dangling bonds and removing the energy levels.

Figure 2.5 illustrates the different recombination mechanisms.

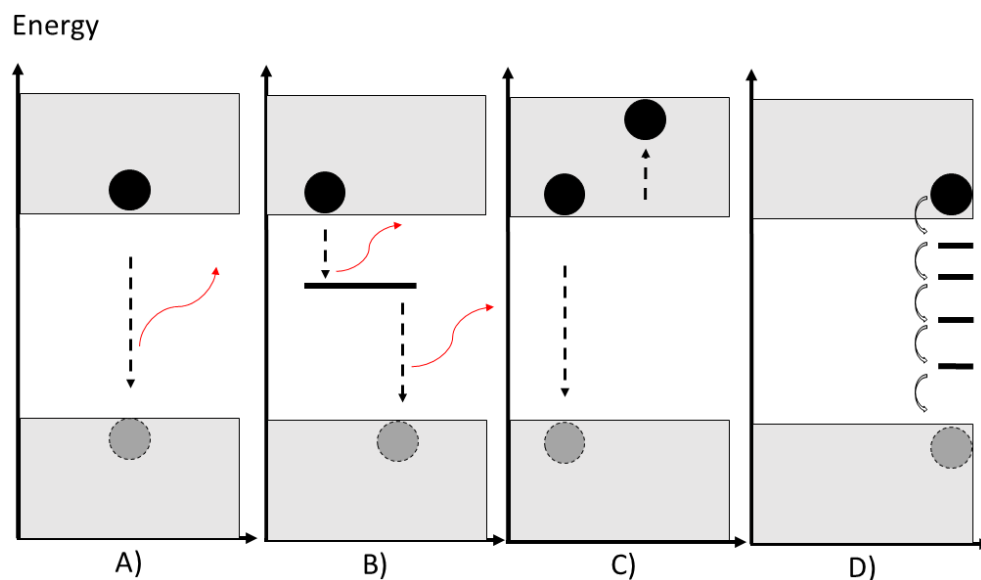


Figure 2.5: Illustration of the primary recombination mechanisms of minority charge carriers in *hpmc-Si* materials. A) Direct radiative recombination. B) Shockley-Read-Hall (SRH) recombination. C) Auger recombination. D) Surface recombination.

#### 2.4.2 Lifetime

The *minority charge carrier lifetime* is the average amount of time a minority charge carrier will exist before recombining. The minority charge carrier is the electron for p-type and the hole for n-type semiconductors. It is the minority carriers that are of interest as they are the limiting factor for conducting an electrical current during illumination. Thus, the efficiency of the cell is greatly dependent on the lifetime; the efficiency increases with lifetime.

## Theory

The recombination mechanisms mentioned in Section 2.4.1 are all in effect in parallel and give rise to the effective minority carrier lifetime,  $\tau_{eff}$ :

$$\frac{1}{\tau_{eff}} = \frac{1}{\tau_{Rad}} + \frac{1}{\tau_{SRH}} + \frac{1}{\tau_{Auger}} + \frac{1}{\tau_{Surf}} + \frac{1}{\tau_{other}} \quad (2.1)$$

$\tau_{Rad}$  is the lifetime due to radiative recombination. It is given by the following equation:

$$\tau_{Rad} = \frac{1}{\beta p_0} \quad (2.2)$$

$\beta$  is a proportionality factor for radiative recombination given hole and electron concentration, and  $p_0$  is the hole concentration under thermal equilibrium for the given p-type semiconductor under low-level injection.

$\tau_{SRH}$  is the lifetime due to SRH recombination and is given by:

$$\tau_{SRH} = \frac{1}{c_n N_T} \quad (2.3)$$

$c_n$  is the *electron capture coefficient* and  $N_T$  is the *trap density* in the p-type semiconductor.

$\tau_{Auger}$  is the lifetime due to Auger recombination. For a strongly doped p-type semiconductor, it is given by:

$$\tau_{Auger} = \frac{1}{C_p N_A^2} \quad (2.4)$$

Where  $C_p$  is a proportionality constant and  $N_A$  is the acceptor concentration.

The terms for surface recombination,  $\tau_{Surf}$ , and other mechanisms,  $\tau_{other}$ , have no simple equations. Surface recombination is detrimental to lifetime when surface passivation is not used and will in those cases dominate the other terms. The “other” term is not of much significance but is included for completeness.

## 2.5 MULTICRYSTALLINE WAFER PRODUCTION AND PROCESSING

Producing mc-Si solar wafers is a long and technical process. This subsection will present the processes most relevant for discussing the findings of this thesis.

### 2.5.1 Casting

To produce silicon wafers molten silicon of high purity is poured into a mould of pure quartz ( $\text{SiO}_2$ ). The high degree of purity of both the silicon and the quartz is important to reduce impurities that would reduce the performance of the wafers (See Section 2.4.1.2). The silicon is then cooled from the bottom and up for the silicon to solidify. It is desirable to have the solidification process go in one direction to take advantage of the difference in solvability of impurities in the molten phase versus the solidified phase. The relationship between the solvability of an impurity in solid phase to the liquid phase is given by the coefficient of segregation,  $k$ :

$$k = \frac{[M_{solid}]}{[M_{liquid}]} \quad (2.5)$$

Where the equilibrium concentration in the solid and liquid is given by  $[M_{solid}]$  and  $[M_{liquid}]$  respectively. For most impurities the value of  $k$  is very small, see Iron and Aluminium in Table 2.1. Therefore, as the silicon solidifies for bottom and up, impurities will be concentrated toward the top, leaving the lower part of the ingot even purer. The impurity rich top can then be removed and discarded. Exceptions from this rule include the dopants boron and phosphorus, as well as the impurity atom oxygen. It is partly the close to unity coefficients of boron and phosphorus that favours them as dopants, for p-type and n-type material respectively, as it is easier to control the doping levels when the dopants distribute somewhat uniformly. As for the oxygen, it will be somewhat concentrated towards the bottom of the ingot and must be dealt with by other means due to the coefficient close to but larger than unity.

Table 2.1: Equilibrium coefficients of segregation,  $k$ , for some impurities and dopants <sup>12</sup>.

	$K$
Iron, Fe	$8.0 \times 10^{-6}$
Aluminium, Al	$2.0 \times 10^{-3}$
Boron, B	0.8
Phosphorus, P	0.35
Oxygen, O	1.25

After solidification, the ingot is sawn into thin, square slices called wafers.

### 2.5.2 Gettering

After casting and cutting (Section 2.5.1), the wafers will still contain some impurities as well as lattice defects. One groups of techniques to further improve the quality of the wafers is called *gettering*. *External gettering* refers to processes that remove impurities or move the impurities to regions were

their effects are of less concern. *Internal gettering* denotes technique that aim to precipitate impurities that are dissolved in the silicon, resulting in regions of lower impurity concentrations. Higher degrees of purity will typically result in lower recombination rates, and thus higher performance of the finished solar cell.

### 2.5.3 Passivation

*Surface passivation* has already been mentioned in Section 2.4.1.4, where dangling bonds on the surface are deactivated by applying a layer that binds to the dangling bonds. Passivation of the bulk material is another technique to further improve the wafer. This is usually, including some samples used for this thesis, done by deposition of a layer of hydrogenated silicon nitride ( $\text{SiN}_x\text{:H}$ ) on the wafers followed by heating to about 400 °C and (simulated) contact firing at 800 °C. The high temperature causes the hydrogen in  $\text{SiN}_x\text{:H}$  to diffuse into the wafer and bond to lattice defects. These defects are related to energy levels in the bandgap, similar to the dangling bonds at the surface of the wafer, which cause recombination. Recombination is in this way reduced.

## 2.6 PHOTOLUMINESCENCE

As mentioned in Section 2.4.1.1 on direct recombination, an electron-hole pair may recombine by releasing a single photon with energy equal to the bandgap. Similarly, SRH recombination (Section 2.4.1.2) may release the same energy in parts, as the electron move through the energy levels. This energy may be released as two or more photons of energies related to the energy levels. These photons, both from direct recombination and SRH recombination, may be collected and their energies used to classify the type of recombination. Classifying the recombination in the wafer may indicate its quality and may be used to improve it or the fabrication techniques.

### 2.6.1 Band-to-Band Photoluminescence

The signal from direct, radiative recombination will be referred to as *band-to-band* (BB) as the electron “jumps” directly from the conduction band to the valence band. A region with high BB signal may indicate a region of high quality, as it indicates that there are few other ways for the charge carriers to recombine. In a situation where the wafer, or cell, is connected to an external circuit, these carriers may have been utilised to do work in the circuit, rather than recombine through the bandgap.

For silicon wafers at 300 K the BB signal will have a wavelength of 1105 nm, equivalent to silicon’s indirect bandgap of 1.12 eV. The signals will from here on be referred to in eV, as is convention in the PV research field.

### 2.6.2 Defect Related Luminescence

The radiative signals from recombination through the energy levels in the bandgap, SRH-recombination, are referred to as *Defect Related Luminescence* (DRL). These signals indicate regions of lower quality and more defects and/or impurities. Signals of different energies are referred to by different names as seen in Table 2.2.

Table 2.2: Different Defect Related Luminescence (DRL) signals and their energy peaks at 4.2 K<sup>13</sup>. The energy peak of D07 is at 90K and read for my data.

Signal	D4	D3	D2	D1	VID3	D07
Energy Peak [eV]	1.000	0.934	0.875	0.812	0.934	0.696

Drozдов et al.<sup>13</sup> was the first to observe DRL in silicon. The signals were called D-lines as the signals where believed to come from dislocations in the silicon sample. The individual signals were called D4 – D1. Other DRL signals, such as VID3<sup>14</sup>, D07 and D5<sup>15</sup>, have been observed later, following a similar naming scheme. As indicated by the name and having the same signal peak D3 and VID3 are somewhat related. They have the same energy but seem to have different origin. D3 can be observed with a weak signal in regions, whereas VID3 has a very strong signal concentrated in points<sup>14</sup>. The name D07 comes from its peak at about 0.7 eV.

### 2.6.3 Defect Related Luminescence as a Function of Temperature

The energy levels in silicon vary with temperature, resulting in a shift in BB and DRL signals. The bandgap of silicon varies from 1.17 eV at 0 K to 1.12 eV at 300 K<sup>16</sup>. This is a result of two effects; phonon availability (see Section 2.1.1) and thermal expansion<sup>17</sup>. A higher temperature causes more phonons to be available for transferring momentum and some energy to the electrons, reducing the bandgap. The thermal expansion expands the crystal lattice, increasing the bond lengths with temperature, which changes the electron energies.

There is a phonon-induced broadening of the signal peaks with increased temperature<sup>18</sup>. It is so as more electron states are suitable for crossing the bandgap when more phonons of different energy and momentum are available. Consequently, the observed peaks in the spectrum are broadened (see Section 3.3.2 for explanation of the spectrum and the B) Figures 4.1 - 4.16 for examples). This motivates imaging at lower temperatures as the signal peaks become sharper and less convoluted.

## 2.7 LIGHT AND ELEVATED TEMPERATURE INDUCED DEGRADATION

Relatively recently a new problem has been of concern to the solar industry: Light and elevated temperature induced degradation.

Among recent improvements to hpmc-Si cells has been the shift from *Aluminium Back Surface Field* cells (Al-BSF) to PERC cells<sup>6</sup>. While having improved performance, the new PERC cells have been found to decrease in performance when put into use. Reductions in performance by as much as 16% has been shown<sup>19</sup>. An improvement is sometimes observed after the degradation low-point is reached, but not necessarily in the cells' lifetime. This leads to substantial losses, even if the cells regenerate. In laboratory conditions, where temperature and illumination can be made higher than in normal use, this degradation and regeneration can be achieved within hours.

LeTID should not be confused with LID (*Light induced degradation*). Where the boron-oxygen (B-O) related LID spans the first 24-48 hours of illumination, and iron-boron-pairs (Fe-B) the first minutes, LeTID develop much slower<sup>6, 20, 21</sup>. LeTID has also been observed in Gallium doped mc-Si, without boron, where the degradation cannot be attributed to B-O or Fe-B<sup>22</sup>.

The mechanism behind LeTID is not fully understood, but it seems to be affected by processing. Two theories have been proposed in literature and is being investigated by the LETuP project<sup>6</sup>: An effect related to metal impurities<sup>23</sup>, and an effect associated with bulk hydrogen<sup>9, 10</sup>. The hydrogen effect will be of most relevance for this experiment as processing related to hydrogen in the samples will be used to varying degree for the different samples. High temperature processes (see simulated contact firing at 800 °C in Section 3.1.1) may introduce more hydrogen from the passivation layer into the bulk of the wafer, passivation defects. The proposed degradation-recovery mechanism involves hydrogen deactivating and reactivating these defects through interactions when the charge carrier density is increased during illumination.

None of the abovementioned theories fully explain the mechanism behind LeTID, but this is where the literature stands. The LeTID effect will be the main topic of this thesis and the following experimental work will describe an experiment on LeTID.



### 3 EXPERIMENTAL

The goal of the section is to provide a thorough description of the methods used in this study. As well as describing the setups and techniques, some theory on the methods will be included. If other sources are not mentioned, the method and setup is highly inspired by Mehl<sup>16</sup> and Burud<sup>8</sup>.

The processing done to the samples at IFE, Norway, will be referred to as pre-processing. The processing done during the experiment will be referred to as processing.

#### 3.1 SAMPLES

The studied samples are high performance multicrystalline silicon (hpmc-Si) sub-wafers provided by IFE, Norway. Two sets of samples, denoted S1 and S2, were examined. The first set contained samples where the surface passivation layer was removed after light soaking. The second set was not light soaked at IFE, nor was the surface passivation removed. See Section 3.1.1 for the full pre-processing schemes. The first letters in “Full Name” in Table 3.1 and Table 3.2 indicate the pre-processing type.

Wafers was selected from different heights of an ingot, denoted by the number in the “Full Name” in Table 3.1 and Table 3.2. For each such standard hpmc-Si wafer at 156mm x 156mm, 9 sub-wafers were cut in a 3 x 3 grid. This cutting and naming scheme is shown in Figure 3.1.

A	B	C
D	E	F
G	H	I

*Figure 3.1: The scheme for cutting and naming the sub-wafers cut from a standard 156 mm x 156 mm hpmc-Si wafer.*

The last letter in the “Full Name” in Table 3.1 and Table 3.2 indicate the placement in this 3 x 3 grid. Four such sub-wafers were chosen as samples for each of the sample sets. For the first set samples S1 A – C were taken from the upper right corner of the wafer. For the second set all the samples were taken from the lower left corner of the wafer.

The number in the “Full Name” in Table 3.1 and Table 3.2 indicate the ingot height of the given sample. For both sets this implies that samples A and B are neighbours and C is almost a neighbour to A and B. This means that A, B and C to a large degree share the same crystal grains and boundaries, leaving room for comparison.



## Experimental

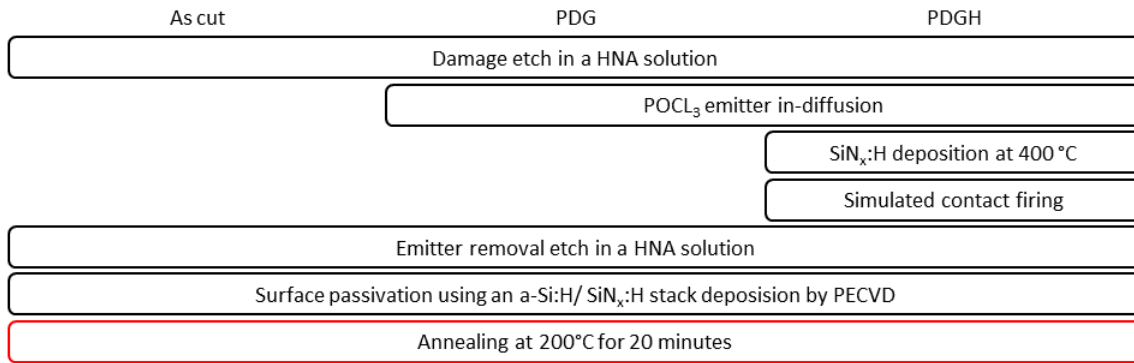


Figure 3.3: Schematic of the pre-processing of the samples in set 2 prior to the main experiment. PECVD stands for Plasma-enhanced chemical vapor deposition.

For sample set 1 A is in the “PDG” column, B in the “as cut” column, and C and D in the “PDGH” column. For sample set 2 A is in the “as cut” column, B in the “PDG” column, and C and D in the “PDGH” column.

The damage etch in an HNA-solution is to remove damages and roughness from the sawing from brick to wafer.

The subsequent POCl<sub>3</sub> emitter in-diffusion is the process which produces the n-region in the wafer, resulting in the p-n junction (Section 2.3). The process also causes *Phosphorus Diffusion Gettering*, PDG, an external gettering process (Section 2.5.2) which increases the purity of the p-region as impurities tend to diffuse toward the phosphorus in the n-region which has a higher solubility for the impurities than the p-region material. The n-region is less susceptible to the negative effects of the additional impurities.

SiN<sub>x</sub>:H deposition combined with simulated contact firing (simulating the application of electrically conduction fingers and busbars on the front of the wafer) causes bulk passivation as hydrogen from SiN<sub>x</sub>:H diffuses into the bulk of the wafers, binding to the imperfections in the lattice. The contact firing is done at 800 °C.

The Emitter removal etch in an HNA-solution removes the n-region, leaving the wafers as a pure p-type again. This remaining p-type material was now very pure, due to the gettering, and was expected to have a long lifetime.

A layer of amorphous Si:H is used for the surface passivation itself, covered by a layer of SiN<sub>x</sub>:H to seal the otherwise unstable a-Si:H.

Sample set 1 was further processed with light soaking at 0.05 suns and room temperature. This was done to activate the degradation associated with light exposure without elevated temperatures; the boron-oxygen (B-O) related LID and iron-boron-pairs (Fe-B)<sup>20, 21</sup>. The light and elevated temperature induced degradation might then be observed later with further processing and imaging. The passivation layer was then removed. SiN<sub>x</sub>:H was first removed in a 5% HF solution, followed by the a-Si:H layer removed in a CP5 solution.

Sample set 2 was annealed at 200 °C for 20 minutes.

## Experimental

Finally, the samples of set 1 and 2 were cleaned in deionized water. The samples were then kept in boxes covered in aluminium foil to block light, as light could cause processes we wanted to observe under controlled circumstances.

### 3.1.2 Processing

Before the samples were processed further, an initial imaging was performed as described in Section 3.2. During imaging the samples were cooled to 90 K, using liquid nitrogen and newly evaporated nitrogen. This is a part of the imaging but is mentioned here for completeness of the treatment of the samples.

The two sets were processed differently, due to their different pre-processing. Sample set 1 was processed with light and elevated temperature: 0.79 suns of light intensity with an AM 1.5 spectrum using a solar simulator, and heated to 150 °C. The processing lasted a total of 17 hours, being interrupted for imaging after 10, 20, 30 and 60 minutes, 2, 5 and 17 hours.

The samples of set 2 were then light soaked at room temperature under 0.23 suns of light intensity with an AM 1.5 spectrum. A UV-filter was used to protect the surface passivation layer (this is done by the glass of the solar panel in a real-life scenario). The light soaking was interrupted by imaging after 16, 21, 41, 64, 65 and 84 hours.

The set 2 samples were then treated with light and elevated temperature: 0.79 suns of light intensity with an AM 1.5 spectrum at 150 °C, still using a UV-filter. This treatment lasted 22 hours, halted for imaging a total of 12 times at uneven intervals: 10, 20, 30 and 60 minutes, 2, 5, 17, 18, 20, 21 and 22 hours.

### 3.2 HYPERSPECTRAL PHOTOLUMINESCENCE IMAGING

The Hyperspectral Photoluminescence Imaging was done with a setup consisting of the hyperspectral camera itself, a line laser for excitation, a long pass filter, a sample holder which is a cryogenic cooler and a cardboard box for frost and fog protection. This equipment was kept inside an aluminium closet where the camera and laser were hung on a rail from the ceiling of the closet while the sample holder was placed on the bottom. The closet was shut during imaging to keep light out. The closet was also anodised and painted black to suppress light reflections. The setup is shown schematically in Figure 3.4:

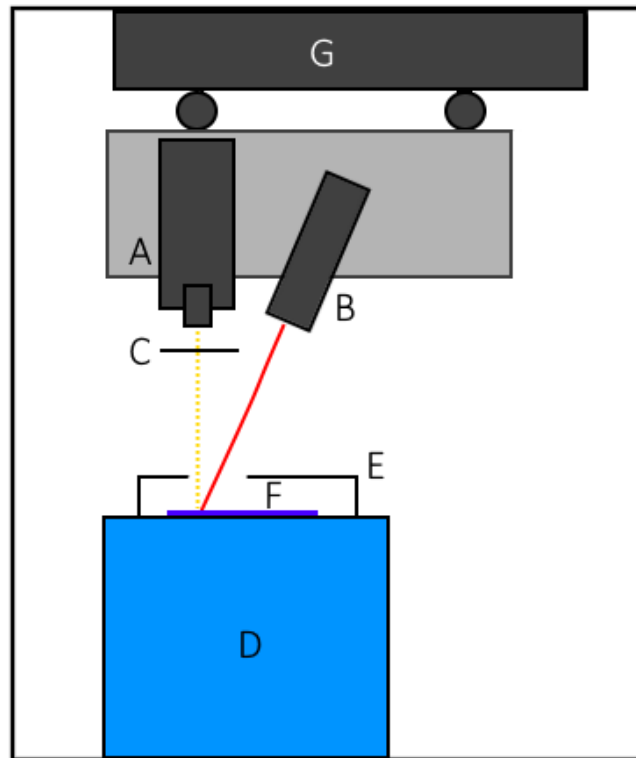


Figure 3.4: Schematic representation of the imaging setup: A) Camera, B) Line laser, C) Long pass filter, D) Sample holder, E) Frost protection, F) The sample and G) Rail for moving the camera (with filter) and laser.

#### 3.2.1 Hyperspectral Camera

The *short wavelength infrared (SWIR) pushbroom* (line scanning) hyperspectral camera used is a model by Specim, Finland (<http://www.specim.fi/>). It uses a HgCdTe CCD-detector with sensitivity in the 929 – 2531 nm wavelength range with resolution varying from 6.32 nm for the shortest wavelength to 6.23 nm for the longest wavelength. This corresponds to the photon energy range 1.33 – 0.49 eV. The different wavelengths are separated as they enter the camera by a diffraction grating. The individual wavelengths are then registered by the CCD at separate pixels.

The camera outputs lines of 320 pixels in width (spatial resolution  $x$ ) for 256 wavelengths (spectral resolution  $\lambda$ ) at 14 bits, yielding values in the range 0 – 16383. As the camera moves over the sample, these lines are combined (for spatial resolution  $y$ ) into what is called a *hypercube*. The hypercube thus has the spatial resolution  $x$ ,  $y$  and spectral resolution  $\lambda$ . The hypercube can be seen as

## Experimental

a stack of images where each image represents the sample as seen by a different wavelength. The length of each image,  $y$ , is set by how many lines are scanned.

The camera was set to an exposure time of 2.5 ms and framerate of 25 Hz. The resolution used was 100  $\mu\text{m}/\text{pixel}$ , which is a result of the distance between the camera and the sample, the lens objective and the internal resolution of the camera. Equation 3.1 is used to calculate the resolution when a picture is taken.

$$\text{resolution} = \frac{N}{x_2 - x_1} \cdot d \quad (3.1)$$

Here  $N$  is the number of electrical contact fingers between pixel number  $x_2$  and pixel number  $x_1$  on a known solar cell with distance  $d$  between each finger.

To keep the same spatial resolution in both  $x$  and  $y$  direction the scanning speed was set to 2.50 mm/s. As seen in Equation 3.2, the scanning speed is the product of the resolution and the framerate  $f$ .

$$\text{scanning speed} = \frac{N}{x_2 - x_1} \cdot d \cdot f \quad (3.2)$$

### 3.2.2 Line Laser

To excite the electron-hole pairs in the sample an 808 nm laser was used. The model is a Lasiris Magnum II from Coherent, USA (<https://www.coherent.com/>). It is a high-power laser diode line generator with an adjustable beam and maximum power of 5600 mW. The wavelength of 808 nm yields a photon energy of 1.53 eV, enough to cross the 1.12 eV bandgap of Si.

### 3.2.3 Long Pass Filter

The reflection of the 808 nm laser will not be detected by the CCD directly, but its 2<sup>nd</sup> order maxima, which is caused by the diffraction grating, will be detected. This signal will coincide with the 1616 nm signal and thus be interpreted as a 1616 nm signal. To prevent this, a long pass filter is placed in front of the camera. The long pass filter blocks radiation of wavelength shorter than 1000 nm, preventing the 808 nm laser from entering the camera. The filter is made by Edmund Optics, USA, (<https://www.edmundoptics.com/>) and is considered a high-performance long pass filter with optical density  $\geq 4$ .

### 3.2.4 Sample Holder/Cryogenic Cooler

The samples were laid on the polished aluminium surface of a cryogenic cooler, cooling it to 90 K (-183 °C). The cooler was an aluminium container filled with liquid nitrogen, isolated with Styrofoam. The aluminium surface is thermally connected to the liquid nitrogen by fins that extend from the surface

## Experimental

inwards, into the liquid nitrogen. The holder also has holes above the sample to allow newly evaporated, cold nitrogen gas to pour over the sample on its way out of the container. To monitor the temperature of the sample a thermometer is attached to the surface of the container.

The samples were cooled as the DRL signals are easier to detect and separate from each other at lower temperatures. See Section 2.6.3.

### 3.2.5 Frost and Fog Protection

As the sample was cooled it tended to collect frozen dew as moist air came in contact with it, preventing clear imaging. Also, frozen water particles in the air above the sample formed a mist, further blurring the image. To prevent this a cardboard box was placed above the sample and a hole was cut to allow the camera to see the sample and the laser to illuminate it, while keeping the airflow near the sample to a minimum.

Frozen dew also tended to accumulate on the surface where the samples were laid for imaging. To minimize this, a sheet was placed on the surface when not in use, and the dew was removed at regular intervals in between imaging.

### 3.3 DATA PROCESSING

The hyperspectral images output from the camera have 256 bands, compared to the usual three red, green and blue bands of ordinary photos. This, combined with the fact that the images are of non-visible light, makes the images unfit for regular viewing. In their raw format the images also contain a high level of noise which preferably should be filtered out. This subsection covers the processing of the images and the visualisation used to interpret them.

The data processing has been done using Python 3.6.4 as distributed by Anaconda (<https://www.anaconda.com/>). The packages used are:

Package	Version
NumPy	1.15.4
Matplotlib	2.2.2
Dill	0.2.9
pyMCR	0.2.1
natsort	6.0.0
SciPy	1.1.0
spectral	0.18
hdf5storage	0.1.15

#### 3.3.1 Pre-Processing

When an image is loaded, background noise is at the same time removed by an algorithm developed by Flø<sup>7</sup> and improved by Mehl<sup>16, 24</sup>. The algorithm has been translated from MATLAB to Python by Marija Vukovic for her PhD. The first step for removing noise is to subtract a dark frame from the raw image. The dark frame is made by recoding some frames with the camera shutter closed after imaging. The dark frame is then constructed as the median of those frames for each pixel. The next step removes noise caused by oscillation in the noise level, originating in the thermal oscillation of the CCD chip due to inconsistent cooling. This is recorded and accounted for by letting the camera run for some minutes after imaging, letting the oscillation reach maximum and minimum. The period is found to be 45 seconds for the camera. This variable noise is then subtracted. The last step is to remove impulse noise, noise caused by temporarily dead pixels, analogue-to-digital conversion errors and bit errors in transmission. This is removed by taking three images in quick succession, all which are corrected by the above steps, and calculating the median of the three images. As the impulse noise is temporal in nature, it will as a rule not be present in more than one image for each combined image pixel. The median image is the fully corrected image, ready for further analysis.

#### 3.3.2 Visualization

To see and interpret the images three types of graphics are generated.



## Experimental

The first graphic is a view of the intensity of the different photon energies recorded in the image. For this, each photon energy level's intensity is summed across the image (the spatial information is discarded). In terms of the hyper cube, all the numbers in each layer of the cube is summed, resulting in a vector of 256 numbers representing the 256 photon energy levels' intensities. These intensities are plotted versus their respective photon energy. This is done for all the images of the same sample to see changes that might occur in the spectrum with processing. For an example, see Figure 4.1 B). This graph gives an overview of the different photon energies that might be of interest for the given sample. The BB signal with a peak around 1.1 eV is of most importance as it is closely related to the minority charge carrier lifetime in the sample, which again is related to the performance and efficiency of the finished solar cell. Other peaks are of interest as they, through Shockley-Read-Hall recombination (Section 2.4.1.2), represent defects in the sample.

The second graphic is a view of the image-wide intensity of the BB signal and its change with heat and light processing. In terms of the hyper cube, for each image of a sample the layers corresponding to the BB signal are summed both in spatial and spectral direction. Which these layers are is known for the camera. Each image is in this way made into one number to give the magnitude of the BB signal across the sample. These numbers are then plotted versus processing time, one for each image of the same sample. For an example, see Figure 4.1 A). This makes it possible to easily see the development in the BB signal as a function of processing time, and by extension see the development in the minority charge carrier lifetime and performance of the sample.

The third graphic is a view of the spatial distribution of intensity of selected photon energies. This looks like a regular image, where the areas of high intensity of the given photon energy is shown in red, while lower intensity fades to dark blue through yellow. The images of a sample are then put next to each other to see the development with processing. See Figure 4.1 C) or Figure 4.17 A) – D) for examples of BB, D3, D2, D1 and D07 figures respectively. As the signals, e. g. BB, consist of several photon energies, the respective layers of the hyper cube are summed in the spectral direction to combine the layers into a single layer to be displayed. This keeps the spatial information of the images.

### 3.3.3 Tools for Spectral Analysis

The signals discussed in the previous section are known from previous studies (see Section 2.6). In an attempt to find new signals, or divide combined signals into its components, a *Multivariate Curve Resolution* (MCR) analysis was performed.

MCR is a method to extract signals from a complex, convoluted dataset. *Principal Component Analysis* (PCA) and *Independent Component Analysis* (ICA) are other alternatives for this. MCR is chosen as it forces the extracted signals to follow physically or chemically meaningful constraints, rather than mathematical or statistical constraints<sup>25</sup>. The MCR algorithm used is the *Multivariate Curve Resolution*

## Experimental

by *Alternating Least Squares* (MCR-ALS) variant. This has been used successfully on hyperspectral images before<sup>8</sup>. The used MCR algorithm for hyperspectral images in Python was written by Marija Vukovic for use in the PV research group at the faculty. The code includes use of the pyMCR Python package and is inspired by the PLS\_Toolbox package for MATLAB.

The MCR method can be mathematically represented as

$$\mathbf{D} = \mathbf{C}\mathbf{S}^T + \mathbf{E} \quad (3.3)$$

Where  $\mathbf{D}$  is the original data, which is decomposed into scores  $\mathbf{S}^T$  and corresponding loadings  $\mathbf{C}$  according to constraints and a user defined number of components. The error matrix  $\mathbf{E}$  represents the difference between the recorded data and the modelled signals. The scores  $\mathbf{S}^T$  give the spatial distribution of the signals in the corresponding loadings  $\mathbf{C}$ , where  $\mathbf{C}$  gives the photon energy of the signals. The error  $\mathbf{E}$  is minimised by the ALS algorithm for MCR-ALS. The result is highly dependent on the number of components; too many will force the algorithm to split the data into too many signals that might not have any physical meaning, while too few will not let the algorithm split the data into its individual signals. A trial-and-error approach has been used to find fitting numbers of components

## 4 RESULTS AND DISCUSSION

---

The following section will present and discuss the results of this endeavour. First the findings for LeTID on the BB signal for non-surface passivated samples will be presented and discussed. The BB signal on the surface passivated samples will follow and be discussed. Then the LeTID effects on DRL signals will be presented and discussed. Finally, an investigation for other signals will be presented in the form of an MCR analysis.

### 4.1 INITIAL ANALYSIS ON NON-SURFACE PASSIVATED SAMPLES

Figures 4.1 - 4.8 will present the initial analysis on the non-surface passivated samples. These are the samples in set 1, denoted S1, that were presented in Section 3.1. The figures and their creation are further explained in Section 3.3.2.

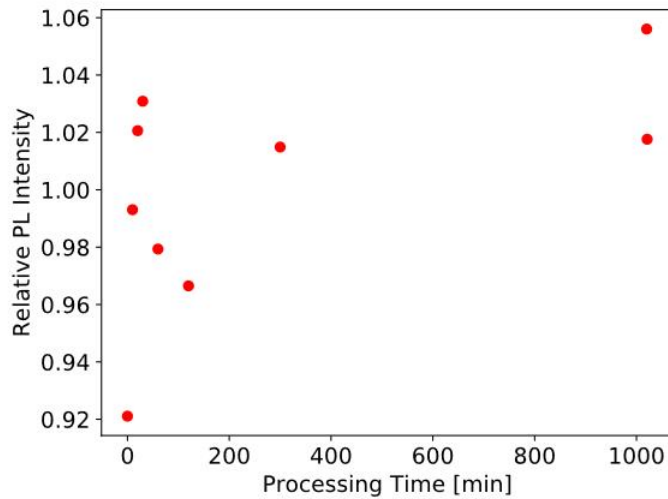
The A) subfigures show the development in the BB signal as a function of processing time. They show a trend towards an increase in signal from the initial measurement to the subsequent measurements. The increase is not consistent with time, but all measurements show a stronger BB signal than the initial measurement. All these recoveries are small however, as seen with a careful inspection of the y-axis, with a maximal change of about 30 percent-points.

The B) subfigures show the magnitude of the different photon energies emitted from the respective samples. They show a small, if any, increase across both BB and DRL signals. A strong BB signal is present with weaker D4 and D3 signals, as well as some other signals between the BB and D4 peaks. An extra strong D4 and D3 signal is seen in Figure 4.7 and Figure 4.8 for a PDGH samples.

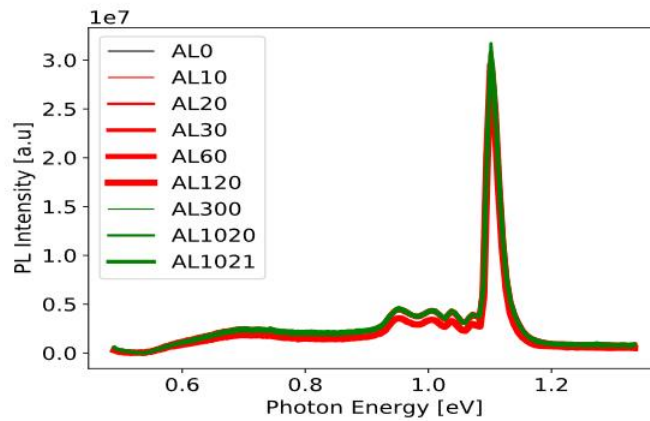
The C) subfigures show the spatial development in the intensity of the BB signal across the respective samples with processing time. They show an increase in the signal in regions. This increase is consistent from the initial to the other measurements, but the intensity does not necessarily increase with the longer processing times. The regions with the biggest change are the regions with an already moderate or high intensity.

## Results and Discussion

A)



B)



C)

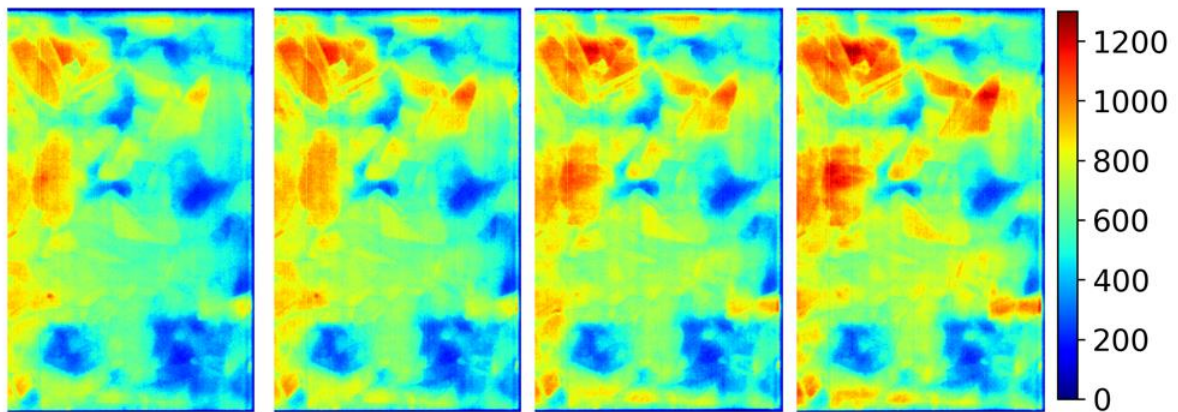
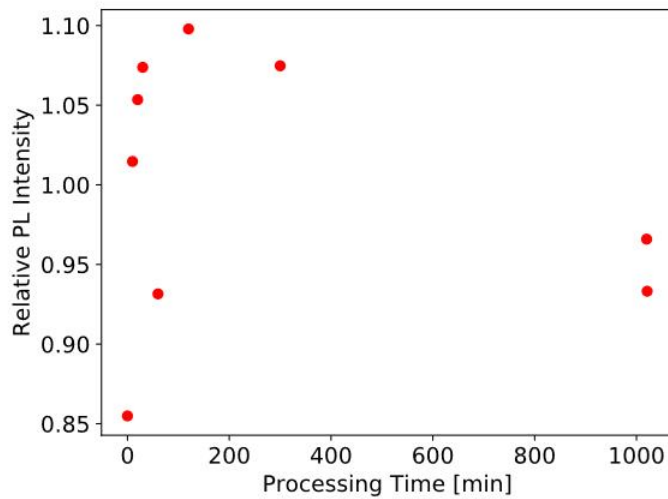


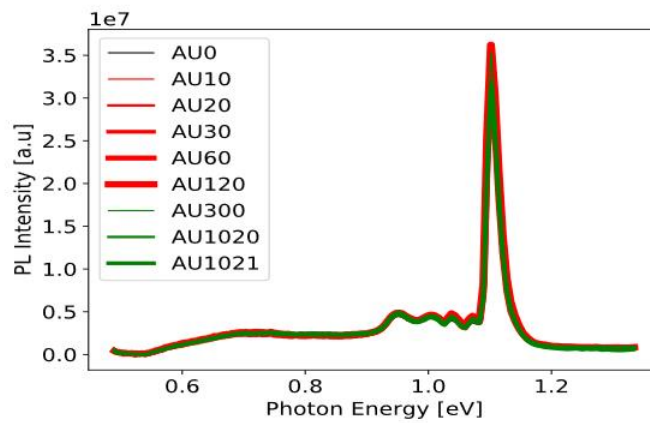
Figure 4.1: Sample S1 AL: Not surface passivated, phosphorus diffusion gettering treated, lower half of sample. A) Relative photoluminescence (PL) intensity integrated over the image for the band-to-band (BB) signal plotted versus processing time (0.79 suns of AM 1.5 at 150 °C). The base for the PL signal is the mean of the intensities. B) PL intensity for the different photon energies at different stages of processing. The number in the legend indicates minutes of processing time for the given line. C) BB signal images for the sample at different processing times: 0, 10, 300 and 1020 minutes of light and heat processing.

## Results and Discussion

A)



B)



C)

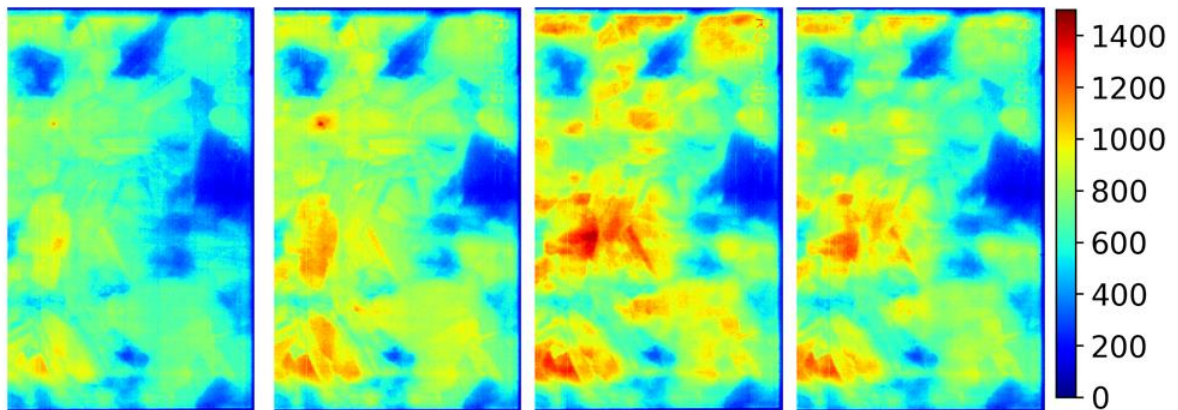
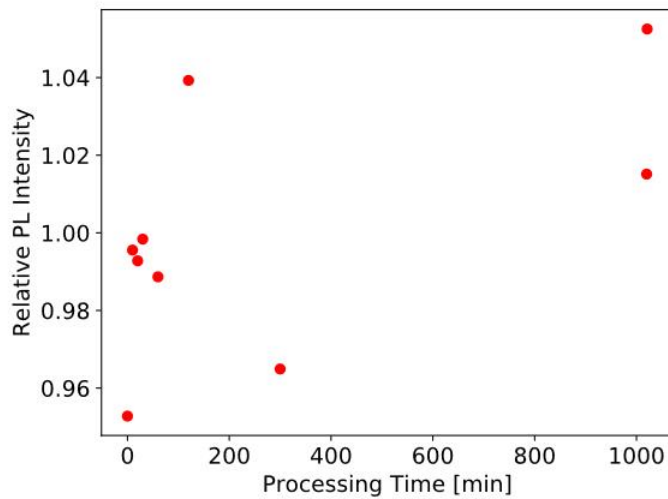


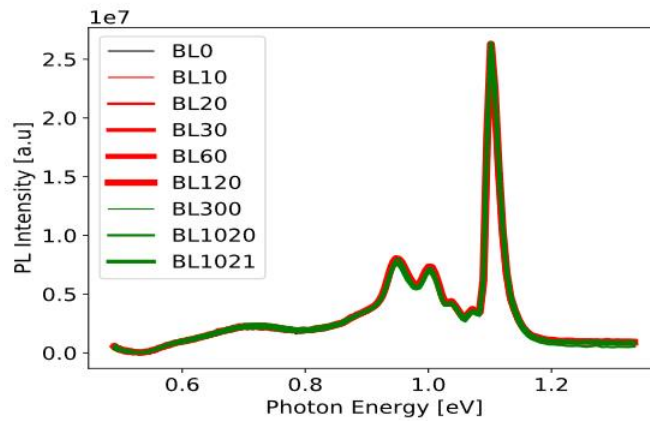
Figure 4.2: Sample S1 AU: Not surface passivated, phosphorus diffusion gettering treated, upper half of sample. A) Relative photoluminescence (PL) intensity integrated over the image for the band-to-band (BB) signal plotted versus processing time (0.79 suns of AM 1.5 at 150 °C). The base for the PL signal is the mean of the intensities. B) PL intensity for the different photon energies at different stages of processing. The number in the legend indicates minutes of processing time for the given line. C) BB signal images for the sample at different processing times: 0, 10, 300 and 1020 minutes of light and heat processing.

## Results and Discussion

A)



B)



C)

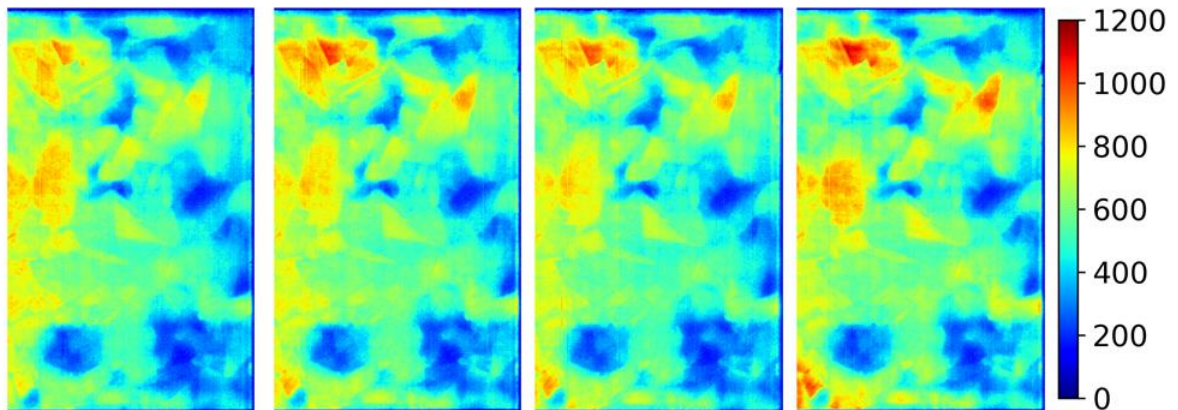
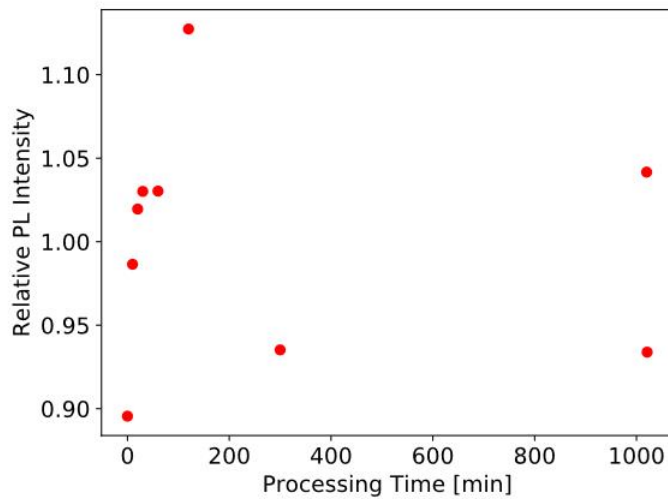


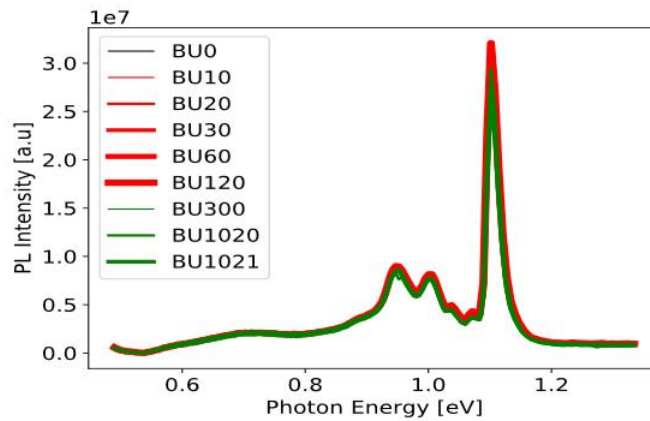
Figure 4.3: Sample S1 BL: Not surface passivated, as cut treated, lower half of sample. A) Relative photoluminescence (PL) intensity integrated over the image for the band-to-band (BB) signal plotted versus processing time (0.79 suns of AM 1.5 at 150 °C). The base for the PL signal is the mean of the intensities. B) PL intensity for the different photon energies at different stages of processing. The number in the legend indicates minutes of processing time for the given line. C) BB signal images for the sample at different processing times: 0, 10, 300 and 1020 minutes of light and heat processing.

## Results and Discussion

A)



B)



C)

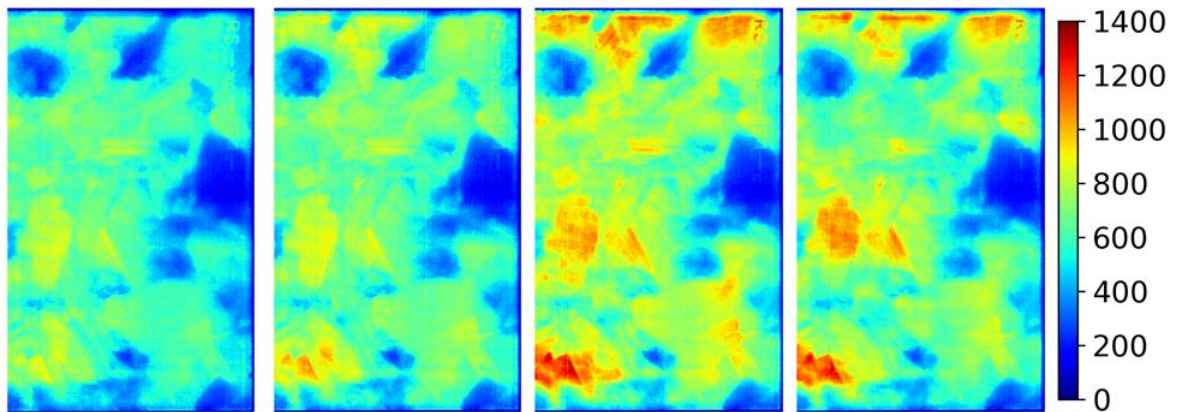
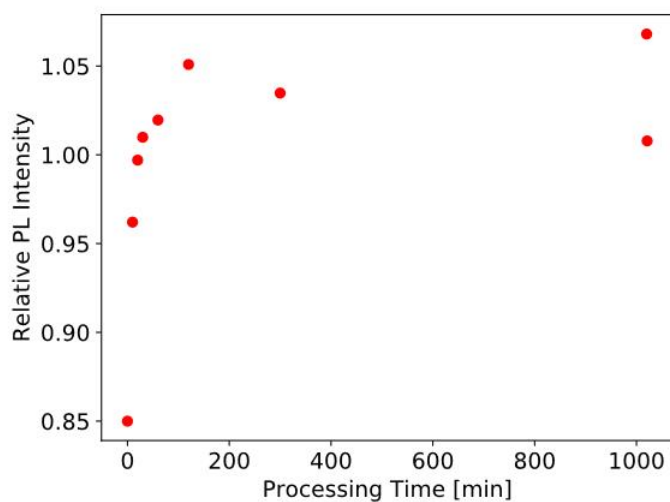


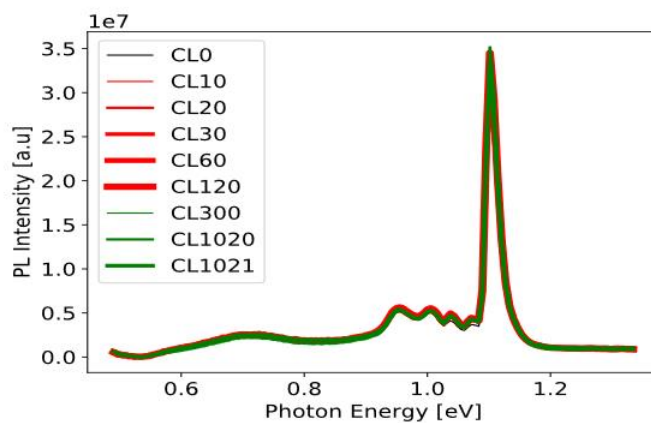
Figure 4.4: Sample S1 BU: Not surface passivated, as cut treated, upper half of sample. A) Relative photoluminescence (PL) intensity integrated over the image for the band-to-band (BB) signal plotted versus processing time (0.79 suns of AM 1.5 at 150 °C). The base for the PL signal is the mean of the intensities. B) PL intensity for the different photon energies at different stages of processing. The number in the legend indicates minutes of processing time for the given line. C) BB signal images for the sample at different processing times: 0, 10, 120 and 1020 minutes of light and heat processing.

## Results and Discussion

A)



B)



C)

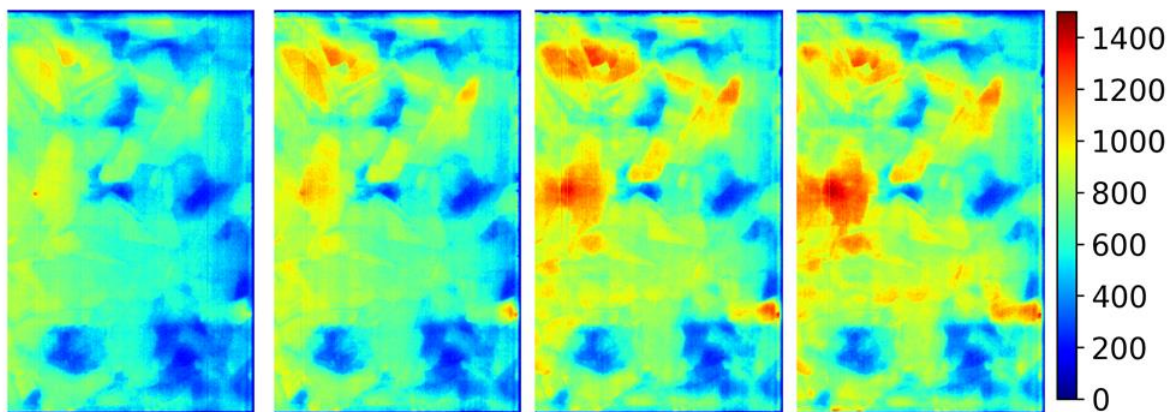
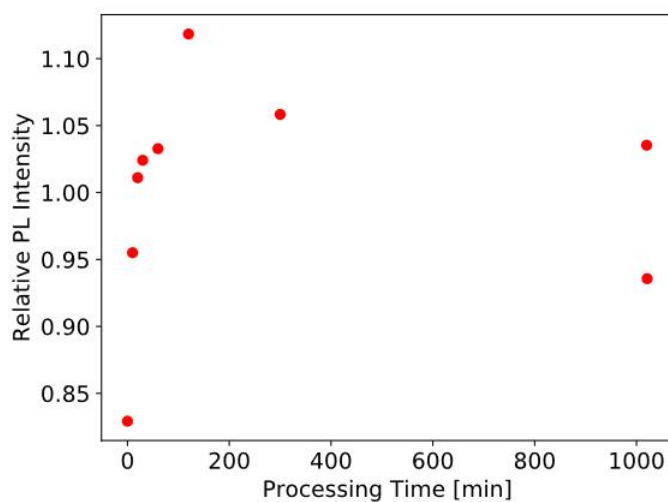


Figure 4.5: Sample S1 CL: Not surface passivated, phosphorus diffusion gettering treated and hydrogen bulk passivated, lower half of sample. A) Relative photoluminescence (PL) intensity integrated over the image for the band-to-band (BB) signal plotted versus processing time (0.79 suns of AM 1.5 at 150 °C). The base for the PL signal is the mean of the intensities. B) PL intensity for the different photon energies at different stages of processing. The number in the legend indicates minutes of processing time for the given line. C) BB signal images for the sample at different processing times: 0, 10, 300 and 1020 minutes of light and heat processing.

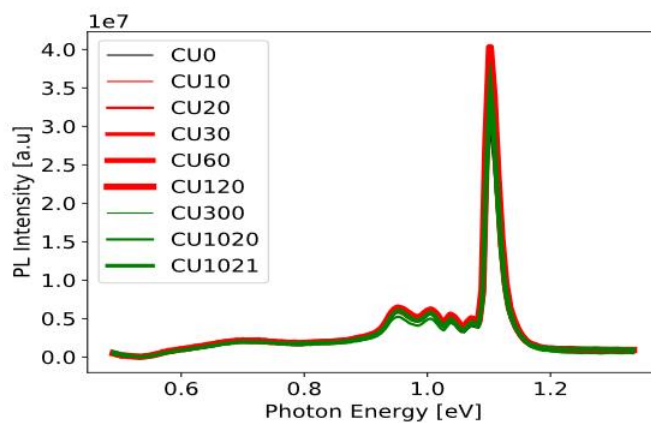


## Results and Discussion

A)



B)



C)

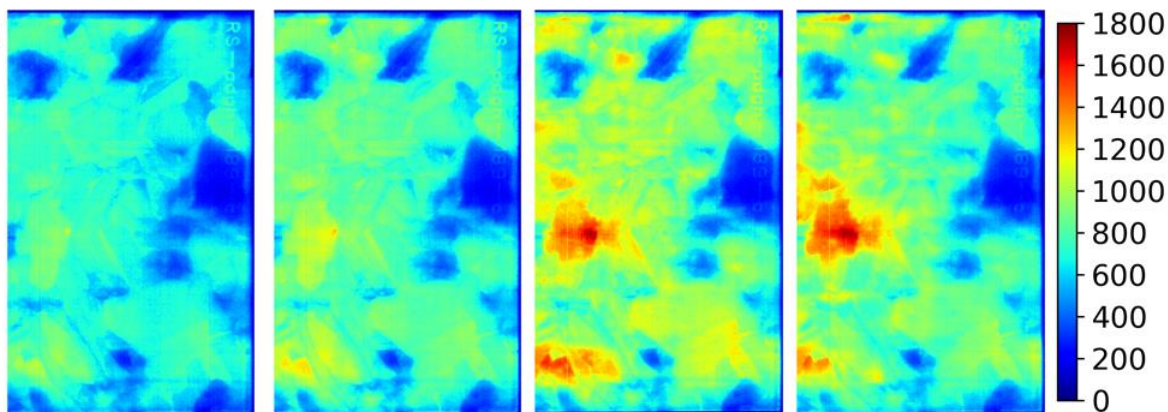
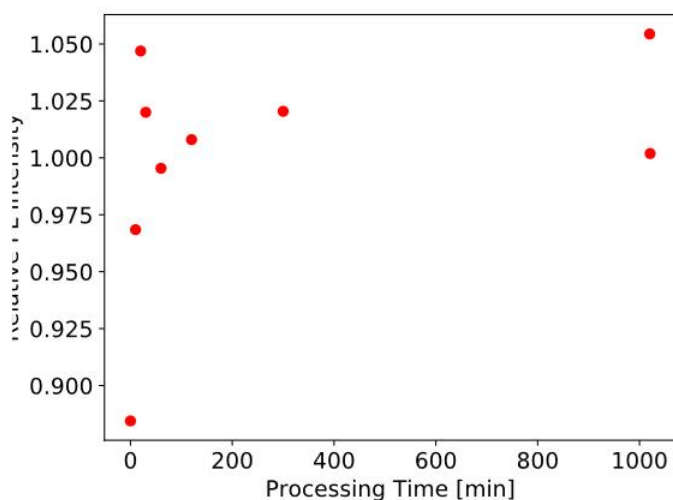


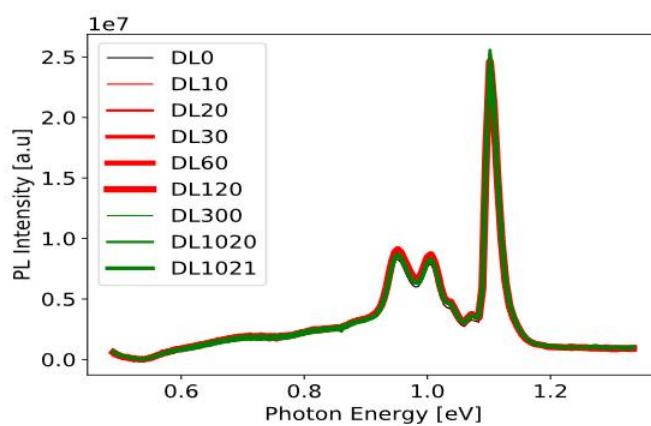
Figure 4.6: Sample S1 CU: Not surface passivated, phosphorus diffusion gettering treated and hydrogen bulk passivated, upper half of sample. A) Relative photoluminescence (PL) intensity integrated over the image for the band-to-band (BB) signal plotted versus processing time (0.79 suns of AM 1.5 at 150 °C). The base for the PL signal is the mean of the intensities. B) PL intensity for the different photon energies at different stages of processing. The number in the legend indicates minutes of processing time for the given line. C) BB signal images for the sample at different processing times: 0, 10, 120 and 1020 minutes of light and heat processing.

## Results and Discussion

A)



B)



C)

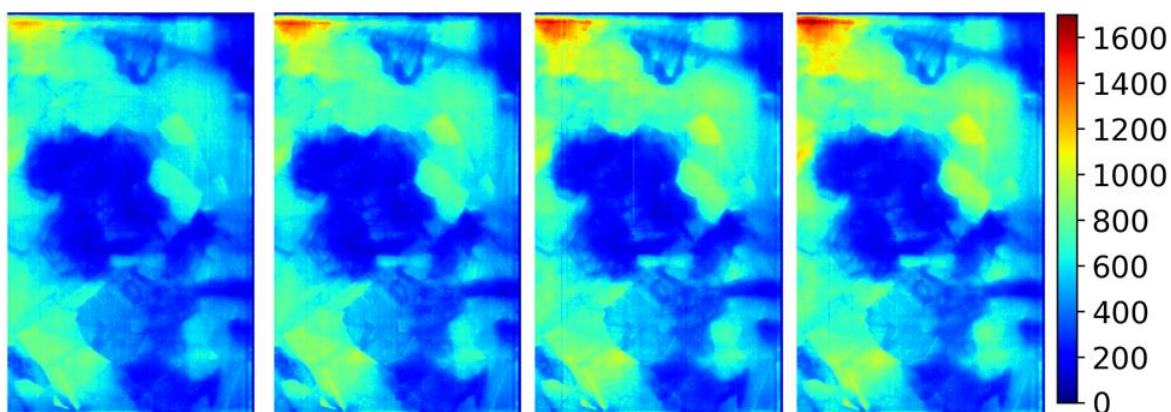
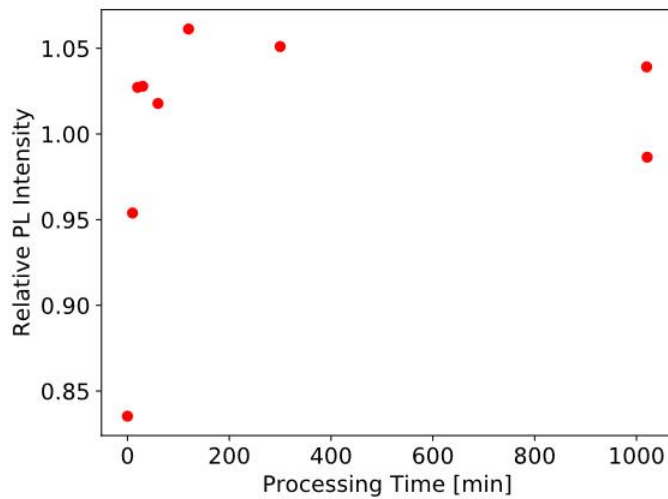


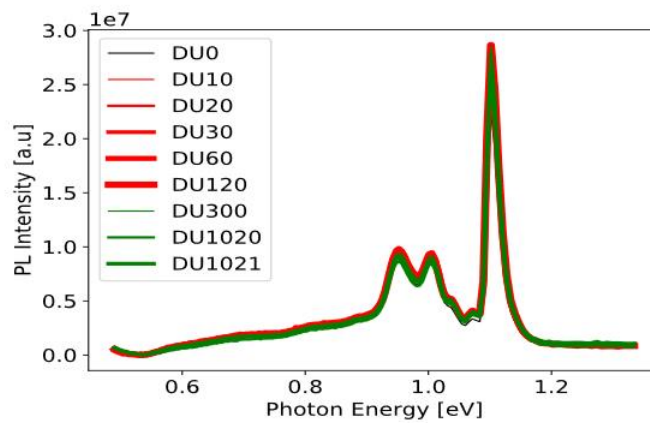
Figure 4.7: Sample S1 DL: Not surface passivated, phosphorus diffusion gettering treated and hydrogen bulk passivated, lower half of sample. A) Relative photoluminescence (PL) intensity integrated over the image for the band-to-band (BB) signal plotted versus processing time (0.79 suns of AM 1.5 at 150 °C). The base for the PL signal is the mean of the intensities. B) PL intensity for the different photon energies at different stages of processing. The number in the legend indicates minutes of processing time for the given line. C) BB signal images for the sample at different processing times: 0, 10, 300 and 1020 minutes of light and heat processing.

## Results and Discussion

A)



B)



C)

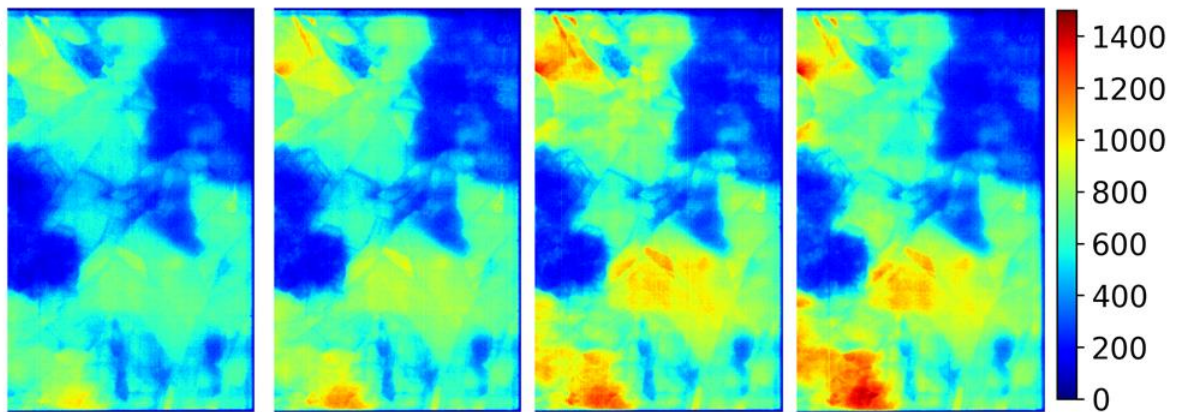


Figure 4.8: Sample S1 DU: Not surface passivated, phosphorus diffusion gettering treated and hydrogen bulk passivated, upper half of sample. A) Relative photoluminescence (PL) intensity integrated over the image for the band-to-band (BB) signal plotted versus processing time (0.79 suns of AM 1.5 at 150 °C). The base for the PL signal is the mean of the intensities. B) PL intensity for the different photon energies at different stages of processing. The number in the legend indicates minutes of processing time for the given line. C) BB signal images for the sample at different processing times: 0, 10, 120 and 1020 minutes of light and heat processing.

The increase in BB signal seen in the A) figures is believed to be caused by a recovery from boron-oxygen (B-O) related LID, as previously presented by Søndena<sup>21</sup>. LID caused by B-O defects is induced by the pre-processing light soak, then recovered by the heat and light processing. The change in signal magnitude is relatively small when compared to the changes observed in the findings where LeTID is present in Section 4.2. This supports the B-O related LID ideal and undermines the presence of LeTID in these samples.

The trend of increasing BB signal with processing, while still present, is harder to observe in the B) figures. These figures however, show slightly increasing or non-decreasing DRL signals. It was expected that DRL signals would decrease when the BB signal increased, but it turns out to not be the case. This was expected as one should expect the DRL signal, the signal of reduced lifetime, to follow the opposite trend of the BB signal, the signal of high lifetime. When the lifetime signal increases, the lifetime reducing signal should decrease, and vice versa. But again, this is not the case. While the BB signal is strong and the D4 and D3 signals are readily observed, some other peaks between the BB and D4 peaks are also present. These signals are believed to be phonon replicas of the BB signal, as is common with a strong BB signal<sup>26</sup>. The extra strong D4 and D3 signals in Figure 4.7 and Figure 4.8, compared to the other figures, is simply caused by the presence of a defect region in the S1 D sample.

The C) figures follow the trend of BB signal increase seen in the A) figures. The observation that the increase from initial to the other observations is consistent support the idea of LID recovery, while the observation that the intensity does not necessarily stabilise with the longer processing times shows that when the recovered state is reached other effects are present, and/or noise is still a concern. The stronger recovery in the already moderate to high BB signal regions suggest that for the LID recovery to be significant, the regions need to be sufficiently defect-free as other defects will conceal the increase in BB signal caused by the recovery.

The observation that there is not degradation induced by the heat and light processing suggests that LeTID does not occur. The small recovery suggests that there were no LeTID present before processing, only LID that recovers with heat and light processing.

This experiment and analysis suggest that surface passivation is of importance for LeTID to occur, as most of the other variables (wafer type, wafer quality, pre-processing, processing) suggest that LeTID should occur in this experiment. This led to the experiment with surface passivated samples, whose findings are presented in the following section.

## 4.2 INITIAL ANALYSIS ON SURFACE PASSIVATED SAMPLES

Figures 4.9 - 4.16 will present the initial analysis on the surface passivated samples. These are the samples in set 2, denoted S2, that were presented in Section 3.1. The figures and their creation are further explained in Section 3.3.2.

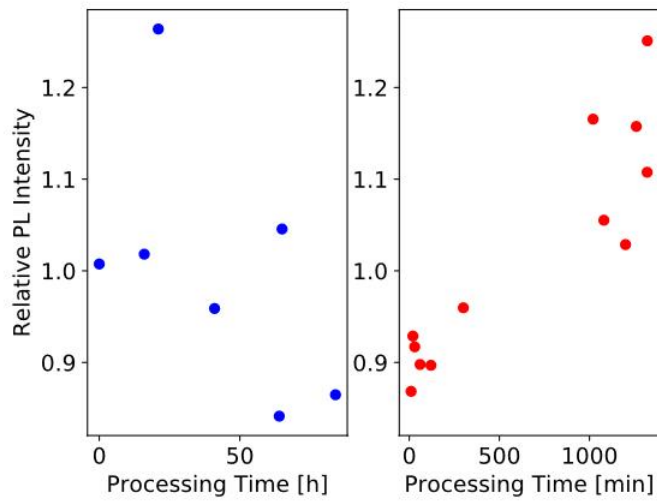
The A) subfigures show the development in the BB signal as a function of processing time. The left of the two subfigures shows the development with light soaking, while the right shows the development with the following light and heat processing. For the as cut and PDG samples, Figures 4.9 - 4.12, the lower signals occur before the light and heat processing, followed by a recovery with light and heat processing. While there are measurements that do not indicate a steady degradation and recovery, the overall trend is still evident. For the PDGH samples, Figures 4.13 - 4.16, there is a decrease in the signal with the light soaking. However, the lowest signals occur within the first measurements of light and heat processing. These minima are followed by a recovery as the light and heat processing continues. For all sample types (as cut, PDG and PDGH), the final measurements often show the same or higher signal levels than the initial measurements.

The B) subfigures show the magnitude of the different photon energies emitted from the respective samples. For all the figures the BB signal is prevalent, together with peaks in the 1.0 and 1.1 eV range. For the as cut samples, Figure 4.9 and Figure 4.10, the D4, D3 and D07 signals are also present. The as cut and PDG samples, Figures 4.9 - 4.12, show the same development in the BB signal as the A) figures, with little or no change for the other photon energies. For the PDGH samples, Figures 4.13 - 4.16, the BB signal mirrors the change seen in the A) figures, with a similar change seen in the peaks between 1.0 and 1.1 eV.

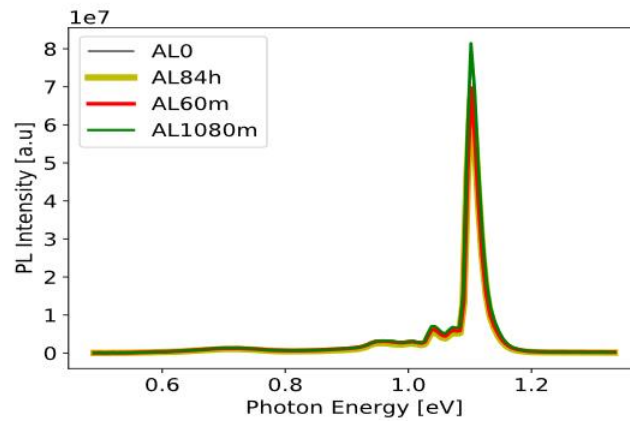
The C) subfigures show the spatial development in the intensity of the BB signal across the respective samples with processing time. The trends seen in the A) figures are also seen there; the as cut and PDG measurements, Figures 4.9 - 4.12, reach their minima after light soaking, while the PDGH measurements, Figures 4.13 - 4.16, degrade further with light and heat processing. The degradations are followed by a recovery with light and heat processing. The regions with an initial moderate to high intensity exhibit the most change, while the regions of low intensity remain so.

## Results and Discussion

A)



B)



C)

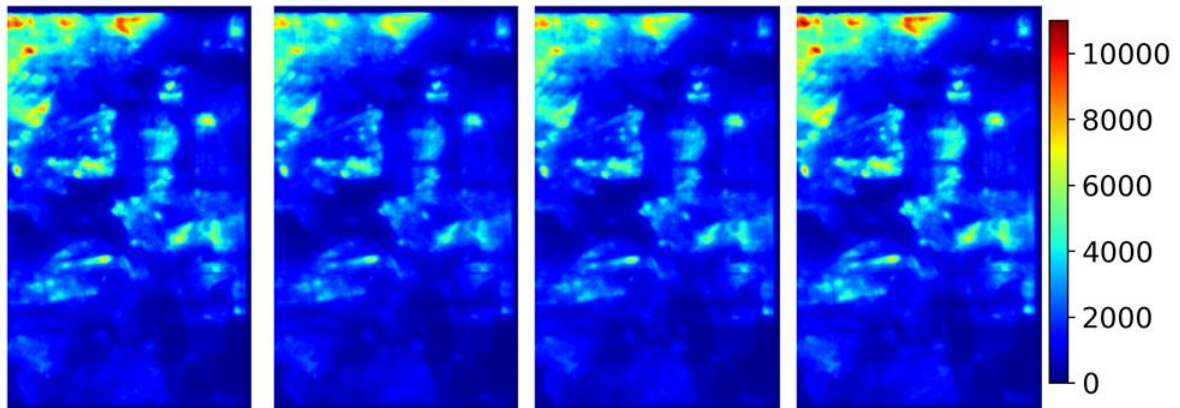
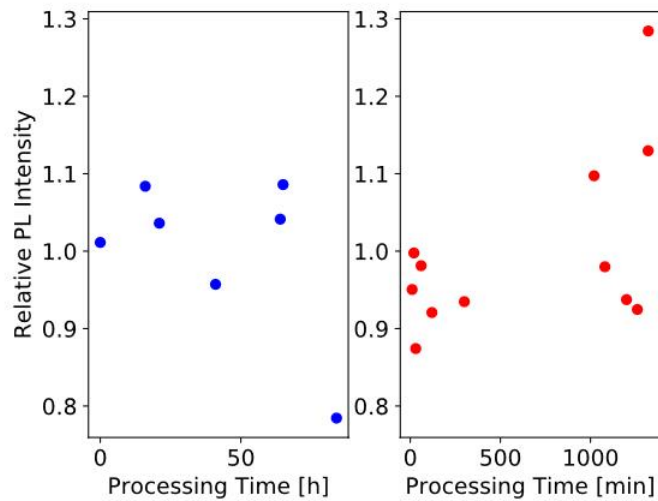


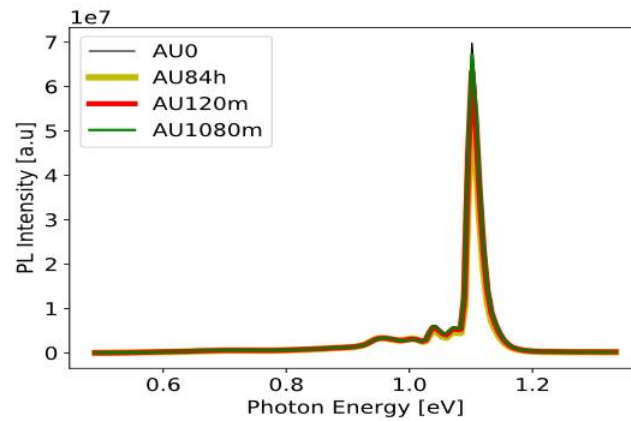
Figure 4.9: Sample S2 AL: Surface passivated, as cut treated, lower half of sample. A) Relative photoluminescence (PL) intensity integrated over the image for the band-to-band (BB) signal plotted versus processing time. For the left window the processing is light soaking at 0.23 suns of AM 1.5. For the right window the processing is light and heat at 0.79 suns of AM 1.5 and 150 °C. The base for the PL signal is the mean of the intensities in the left window. B) PL intensity for the different photon energies at different stages of processing. The number in the legend indicates processing time for the given line, “h” indicating hours of light soaking and “m” indicating minutes of light and heat processing. C) BB signal images for the sample at different processing times: initial (0), 84 hours of light soaking, 60 and 1080 minutes of light and heat treatment.

## Results and Discussion

A)



B)



C)

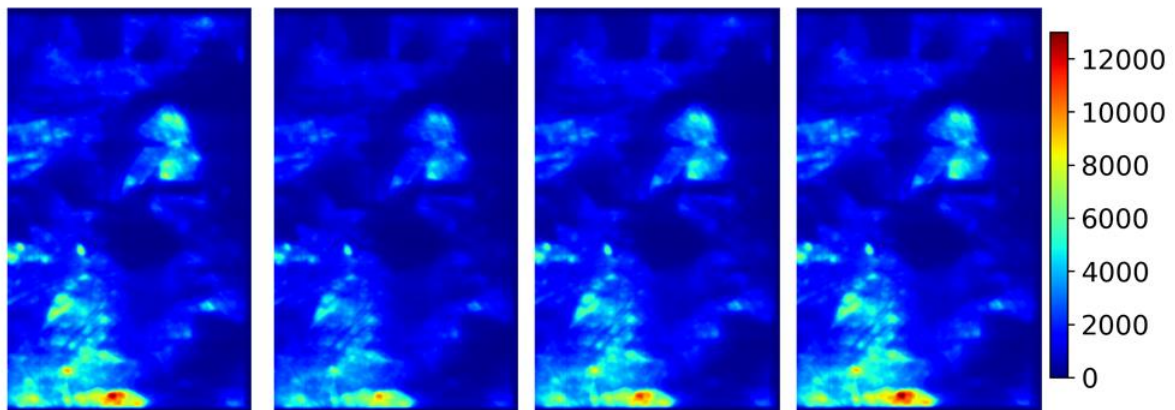
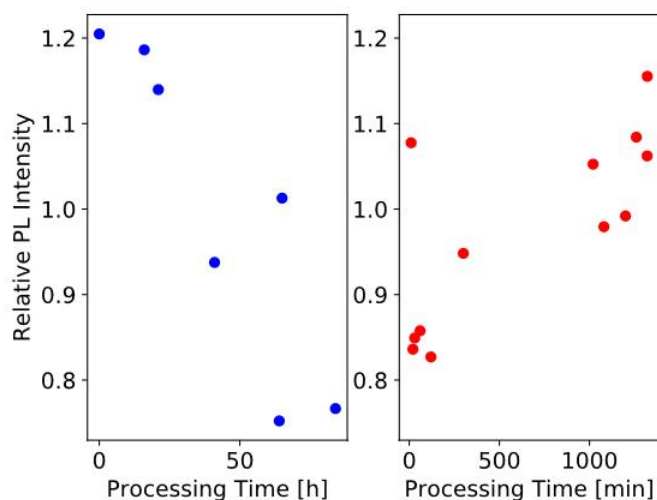


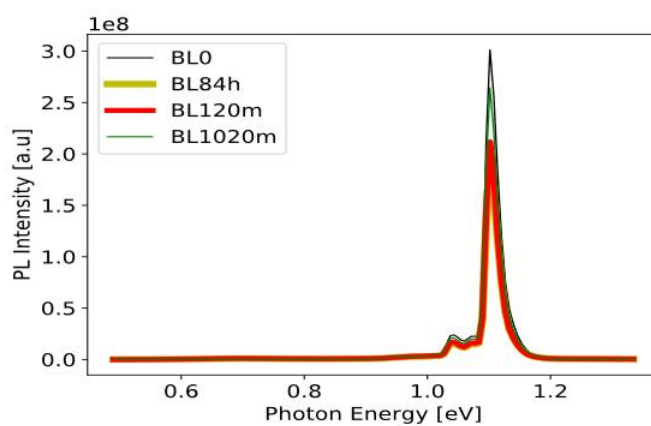
Figure 4.10: Sample S2 AU: Surface passivated, as cut treated, upper half of sample. A) Relative photoluminescence (PL) intensity integrated over the image for the band-to-band (BB) signal plotted versus processing time. For the left window the processing is light soaking at 0.23 suns of AM 1.5. For the right window the processing is light and heat at 0.79 suns of AM 1.5 and 150 °C. The base for the PL signal is the mean of the intensities in the left window. B) PL intensity for the different photon energies at different stages of processing. The number in the legend indicates processing time for the given line, "h" indicating hours of light soaking and "m" indicating minutes of light and heat processing. C) BB signal images for the sample at different processing times: initial (0), 84 hours of light soaking, 120 and 1080 minutes of light and heat treatment.

## Results and Discussion

A)



B)



C)

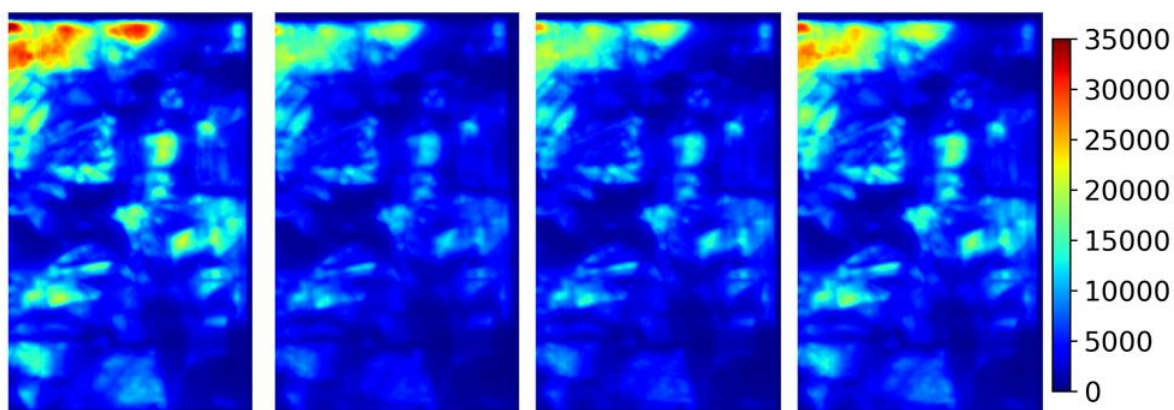
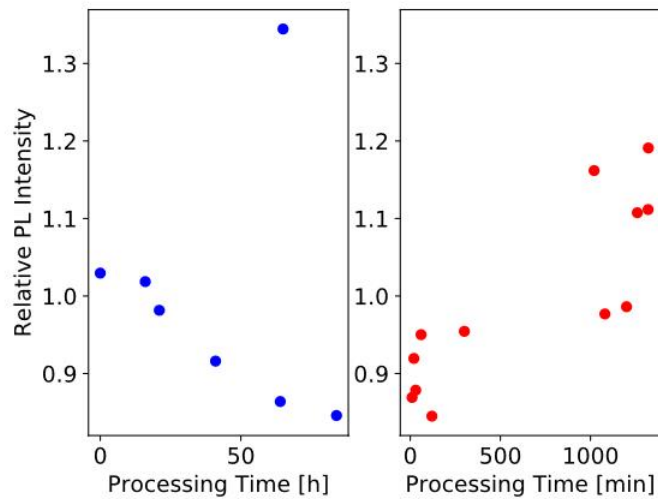


Figure 4.11: Sample S2 BL: Surface passivated, phosphorus diffusion gettering treated, lower half of sample. A) Relative photoluminescence (PL) intensity integrated over the image for the band-to-band (BB) signal plotted versus processing time. For the left window the processing is light soaking at 0.23 suns of AM 1.5. For the right window the processing is light and heat at 0.79 suns of AM 1.5 and 150 °C. The base for the PL signal is the mean of the intensities in the left window. B) PL intensity for the different photon energies at different stages of processing. The number in the legend indicates processing time for the given line, “h” indicating hours of light soaking and “m” indicating minutes of light and heat processing. C) BB signal images for the sample at different processing times: initial (0), 84 hours of light soaking, 120 and 1020 minutes of light and heat treatment.

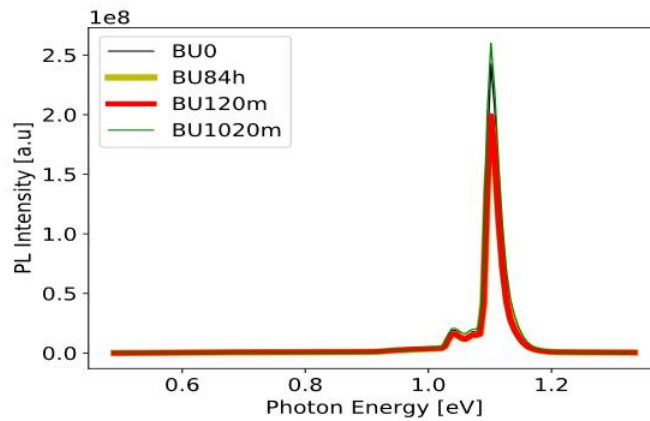


## Results and Discussion

A)



B)



C)

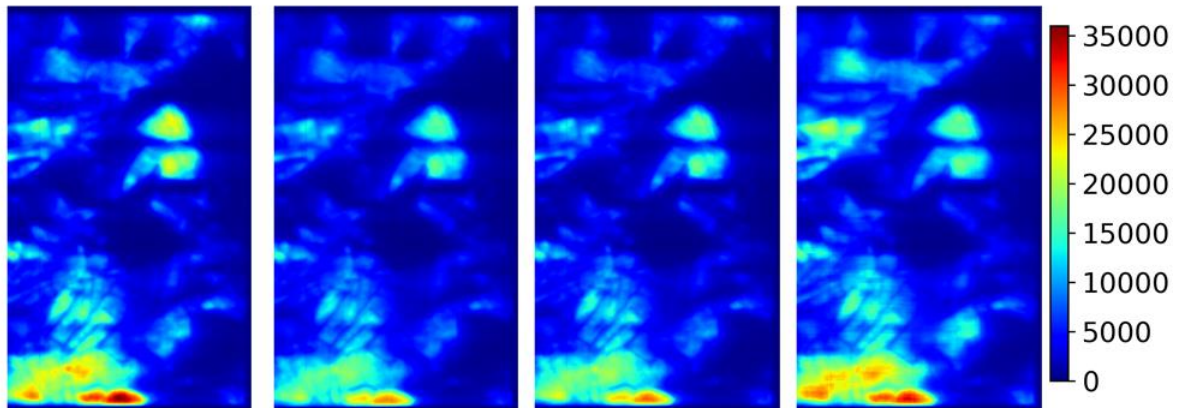
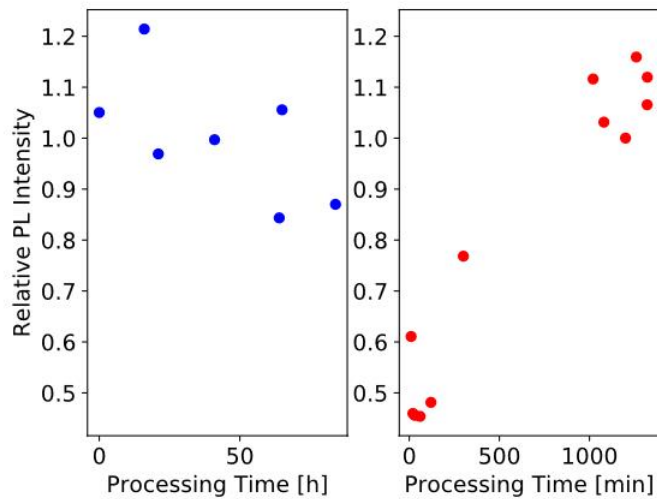


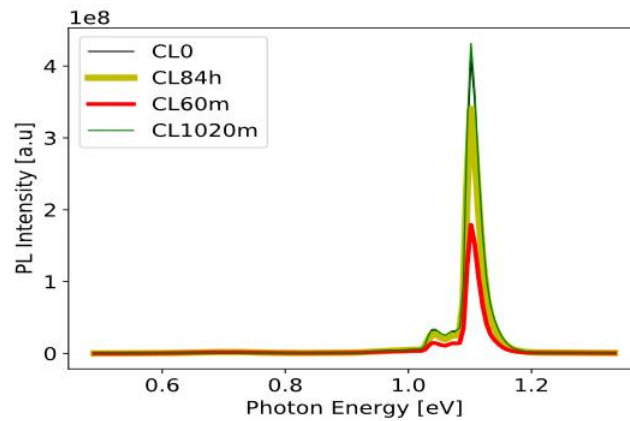
Figure 4.12: Sample S2 BU: Surface passivated, phosphorus diffusion gettering treated, upper half of sample. A) Relative photoluminescence (PL) intensity integrated over the image for the band-to-band (BB) signal plotted versus processing time. For the left window the processing is light soaking at 0.23 suns of AM 1.5. For the right window the processing is light and heat at 0.79 suns of AM 1.5 and 150 °C. The base for the PL signal is the mean of the intensities in the left window. B) PL intensity for the different photon energies at different stages of processing. The number in the legend indicates processing time for the given line, “h” indicating hours of light soaking and “m” indicating minutes of light and heat processing. C) BB signal images for the sample at different processing times: initial (0), 84 hours of light soaking, 120 and 1020 minutes of light and heat treatment.

## Results and Discussion

A)



B)



C)

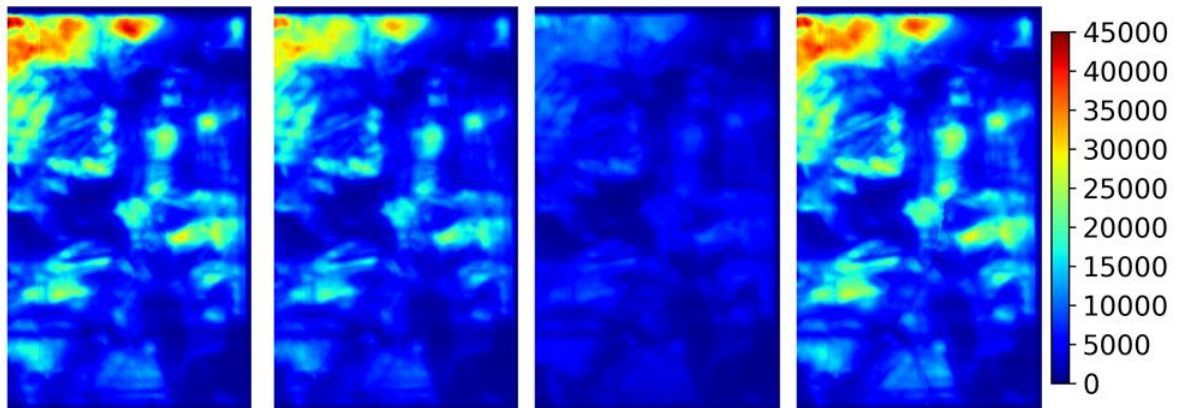
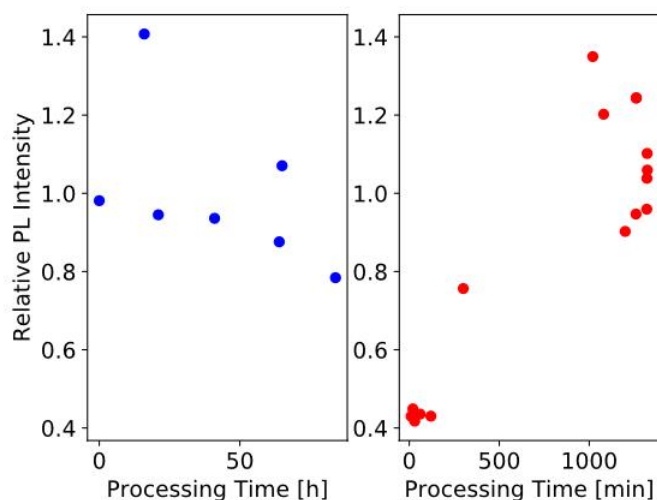


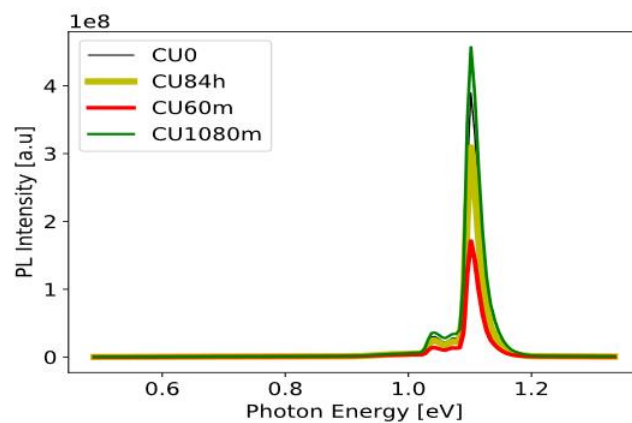
Figure 4.13: Sample S2 CL: Surface passivated, phosphorus diffusion gettering treated and hydrogen bulk passivated, lower half of sample. A) Relative photoluminescence (PL) intensity integrated over the image for the band-to-band (BB) signal plotted versus processing time. For the left window the processing is light soaking at 0.23 suns of AM 1.5. For the right window the processing is light and heat at 0.79 suns of AM 1.5 and 150 °C. The base for the PL signal is the mean of the intensities in the left window. B) PL intensity for the different photon energies at different stages of processing. The number in the legend indicates processing time for the given line, “h” indicating hours of light soaking and “m” indicating minutes of light and heat processing. C) BB signal images for the sample at different processing times: initial (0), 84 hours of light soaking, 60 and 1020 minutes of light and heat treatment.

## Results and Discussion

A)



B)



C)

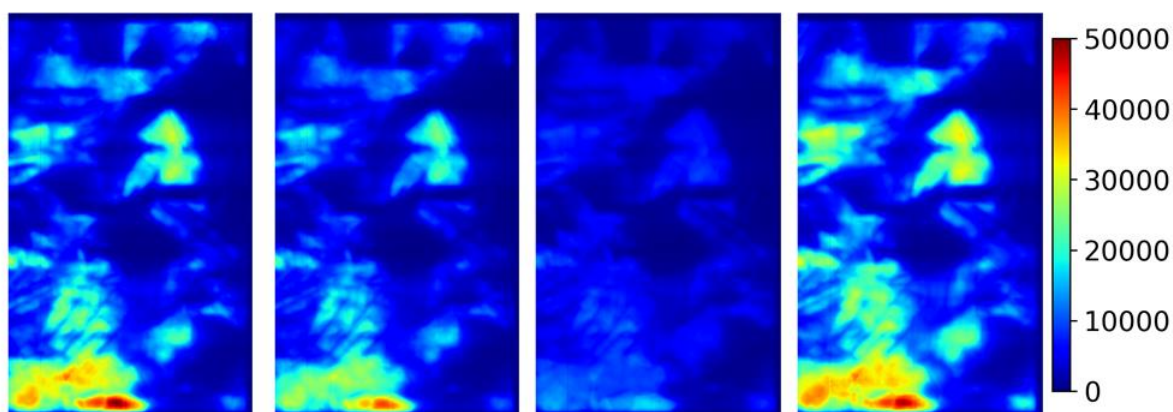
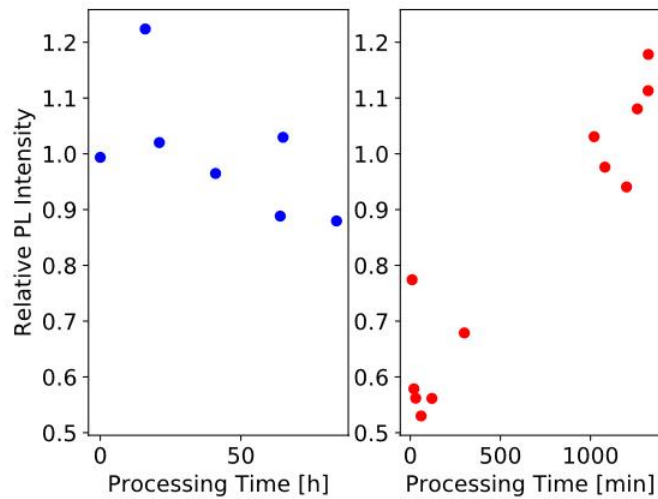


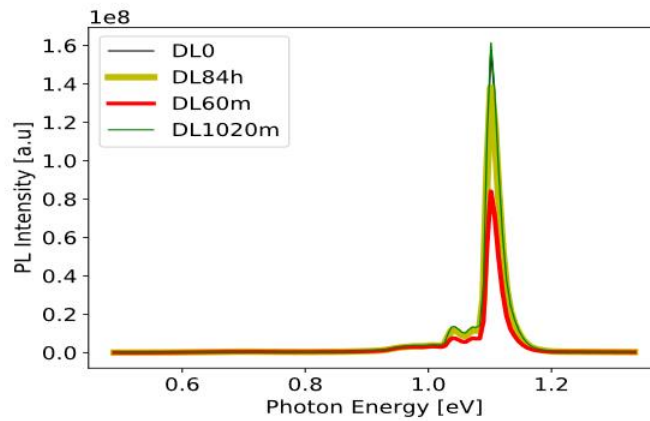
Figure 4.14: Sample S2 CU: Surface passivated, phosphorus diffusion gettering treated and hydrogen bulk passivated, upper half of sample. A) Relative photoluminescence (PL) intensity integrated over the image for the band-to-band (BB) signal plotted versus processing time. For the left window the processing is light soaking at 0.23 suns of AM 1.5. For the right window the processing is light and heat at 0.79 suns of AM 1.5 and 150 °C. The base for the PL signal is the mean of the intensities in the left window. B) PL intensity for the different photon energies at different stages of processing. The number in the legend indicates processing time for the given line, “h” indicating hours of light soaking and “m” indicating minutes of light and heat processing. C) BB signal images for the sample at different processing times: initial (0), 84 hours of light soaking, 60 and 1080 minutes of light and heat treatment.

## Results and Discussion

A)



B)



C)

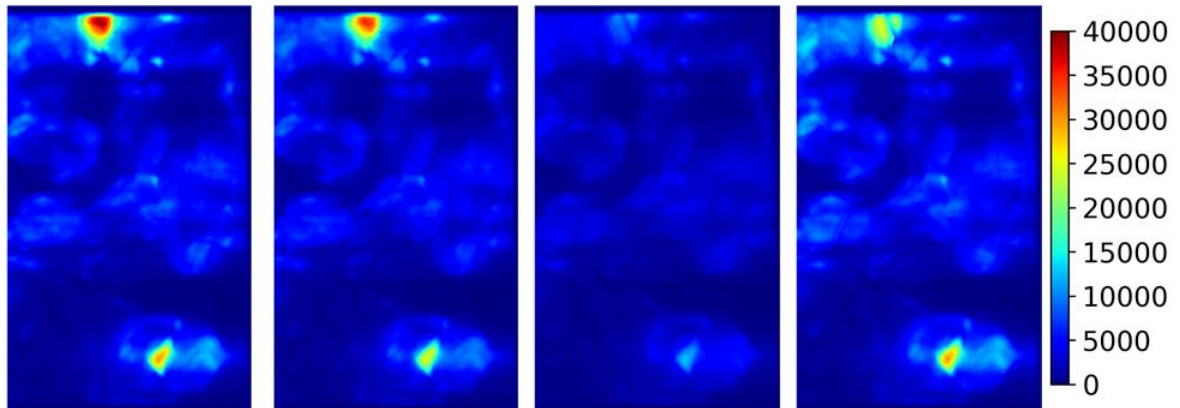
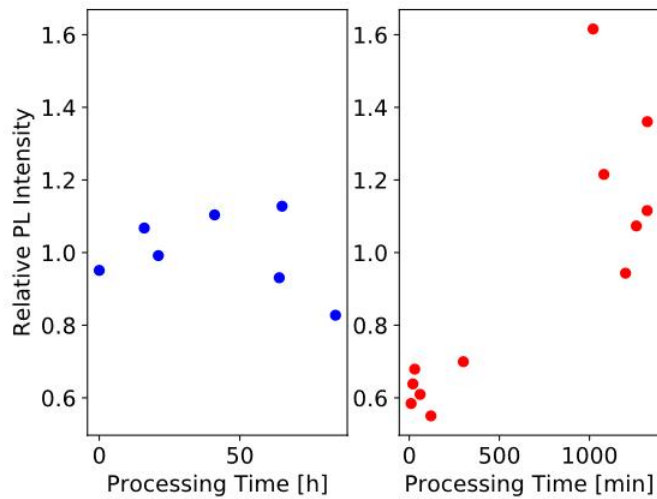


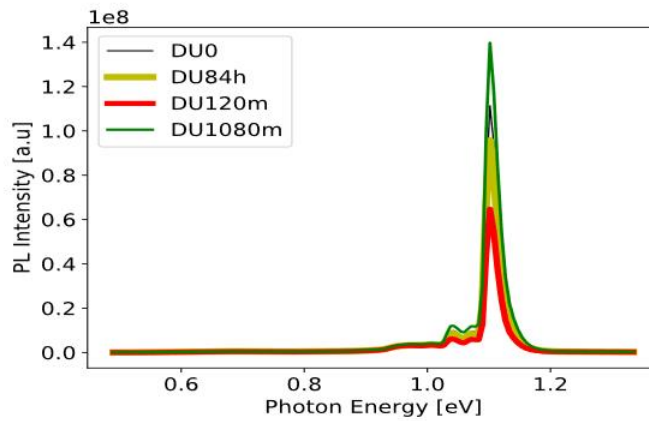
Figure 4.15: Sample S2 DL: Surface passivated, phosphorus diffusion gettering treated and hydrogen bulk passivated, lower half of sample. A) Relative photoluminescence (PL) intensity integrated over the image for the band-to-band (BB) signal plotted versus processing time. For the left window the processing is light soaking at 0.23 suns of AM 1.5. For the right window the processing is light and heat at 0.79 suns of AM 1.5 and 150 °C. The base for the PL signal is the mean of the intensities in the left window. B) PL intensity for the different photon energies at different stages of processing. The number in the legend indicates processing time for the given line, “h” indicating hours of light soaking and “m” indicating minutes of light and heat processing. C) BB signal images for the sample at different processing times: initial (0), 84 hours of light soaking, 60 and 1020 minutes of light and heat treatment.

## Results and Discussion

A)



B)



C)

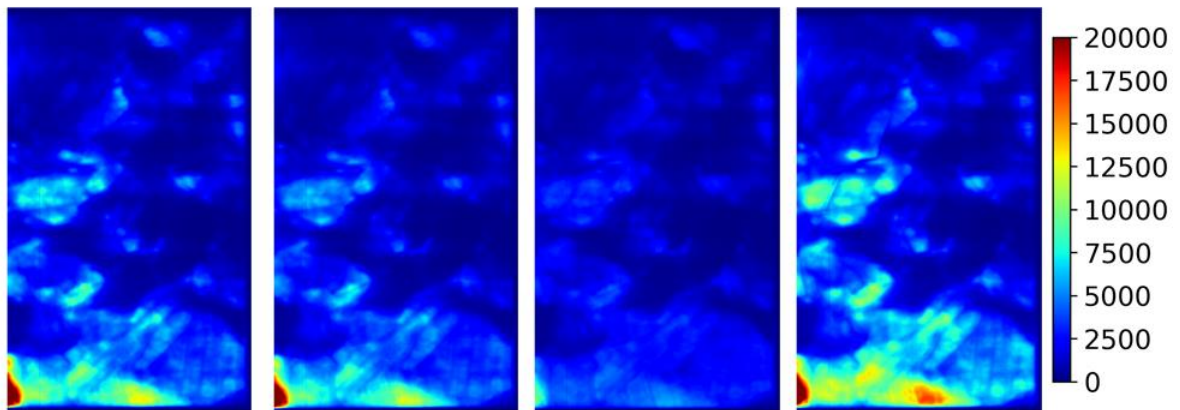


Figure 4.16: Sample S2 DU: Surface passivated, phosphorus diffusion gettering treated and hydrogen bulk passivated, upper half of sample. A) Relative photoluminescence (PL) intensity integrated over the image for the band-to-band (BB) signal plotted versus processing time. For the left window the processing is light soaking at 0.23 suns of AM 1.5. For the right window the processing is light and heat at 0.79 suns of AM 1.5 and 150 °C. The base for the PL signal is the mean of the intensities in the left window. B) PL intensity for the different photon energies at different stages of processing. The number in the legend indicates processing time for the given line, “h” indicating hours of light soaking and “m” indicating minutes of light and heat processing. C) BB signal images for the sample at different processing times: initial (0), 84 hours of light soaking, 120 and 1080 minutes of light and heat treatment.

## Results and Discussion

The as cut and PDG samples in the A) figures does not seem to be affected by the LeTID effect as the lowest signals are reached before the light and heat processing. The recovery seen with the light and heat processing resembles the recovery seen in the non-surface passivated samples discussed in Section 4.1. Therefore, the as cut and PDG samples seem to be affected by the same B-O related LID effect that affected the non-surface passivated samples. The measurements at the light soaked states show the LID develop.

The PDGH samples in the A) figures show the same degradation with light soaking as the other samples, which is assumed to be caused by the same B-O related LID. However, further degradation as the light and heat processing starts indicates the LeTID effect we are looking for. These low signals are reached within the first 2 hours of light and heat processing, before the recoveries follow. Similar development has been shown earlier in lifetime measurements<sup>27</sup>. As only the surface passivated PDGH samples show this degradation it indicates that both a high hydrogen level and charge carrier density are prerequisites for the LeTID to occur. The LeTID did not affect the samples without surface passivation, which have low charge carrier density, nor the as cut and PDG samples, which are not bulk passivated by diffused hydrogen.

All the samples in the B) figures show a strong BB signal together with other peaks in the 1.0 to 1.1 eV range, assumed to be BB phonon replicas. Strong BB signals, with associated replicas, are expected as these samples are of high purity, and now with surface passivation. The D4, D3 and D07 signals present in the as cut samples, that are not present in the other samples, may be a result of the samples not been PDG-processed, as the other sample are to increase their purity. The PDG and PDGH samples B and C are neighbours to the as cut samples A and should thus to a large extent share the same defects, were it not for the processing. All samples show change in the BB signal with processing, following the trend of degradation and recovery seen in the A) figures, showing LeTID for the PDGH samples and not for the rest. This makes the PDGH samples have a bigger change with processing. The change in the BB phonon replicas of the PDGH samples may be a result of the big changes in the BB signal, while this change is not seen for the other samples as the change in BB signal is smaller.

The LeTID effect is again seen in the C) figures for the PDGH samples and not for the as cut and PDG samples. The bigger changes in intensity in the regions of moderate to high intensity suggest that for the LID and LeTID effects to be significant, the regions need to be of sufficiently high purity and defect freeness as impurities and defects would conceal the effects by rendering the BB signal too low to be further decreased significantly.

### 4.3 FURTHER ANALYSIS ON THE SURFACE AND BULK PASSIVATED SAMPLES

Figures 4.17 - 4.20 will present a further analysis on the surface and bulk passivated samples, regarding defect related luminescence. These are the samples that seemed to be affected by the LeTID-effect when examined in Section 4.1 and 4.2; S2 – CL, CU, DL and DU. Here they are examined in a similar fashion to the C) figures in the previous sections, the spatial expanse is in focus, but this time for the DRL signals D3, D2, D1 and D07. The images are selected, from left to right, so that the first is of the initial state, the second of the degraded state (degraded BB signal) before light and heat processing, the third of the degraded state with light and heat processing, and the fourth of the recovered state after long light and heat processing.

The A) figures, the D3 signal, show a decrease with the second and third image, before an increase with the fourth image. This degradation and recovery are seen in both points, lines and regions. No points, lines or regions appear or disappear, only the intensity of those already present change.

The B) figures, the D2 signal, follow the same pattern of degradation and recovery as the D3 signal, if to a lesser extent. The degradation and recovery are seen in points and lines, and to a lesser extent in region. Points, lines and regions still only change intensity, and does not disappear or appear.

The C) and D) figures, of the D1 and D07 signals respectively, too show the trend of degradation, degradation and recovery, but still to a lesser extent than the D3 signal and the BB signal. Here the signals appear as points and lines, but not in regions. The points and lines change intensity but does not appear or disappear. Some of the D07 images have been enhanced to show a high degree of saturation to make the less intense points visible. This may give the impression of large regions of D07 signal, but this is not the case.

## Results and Discussion

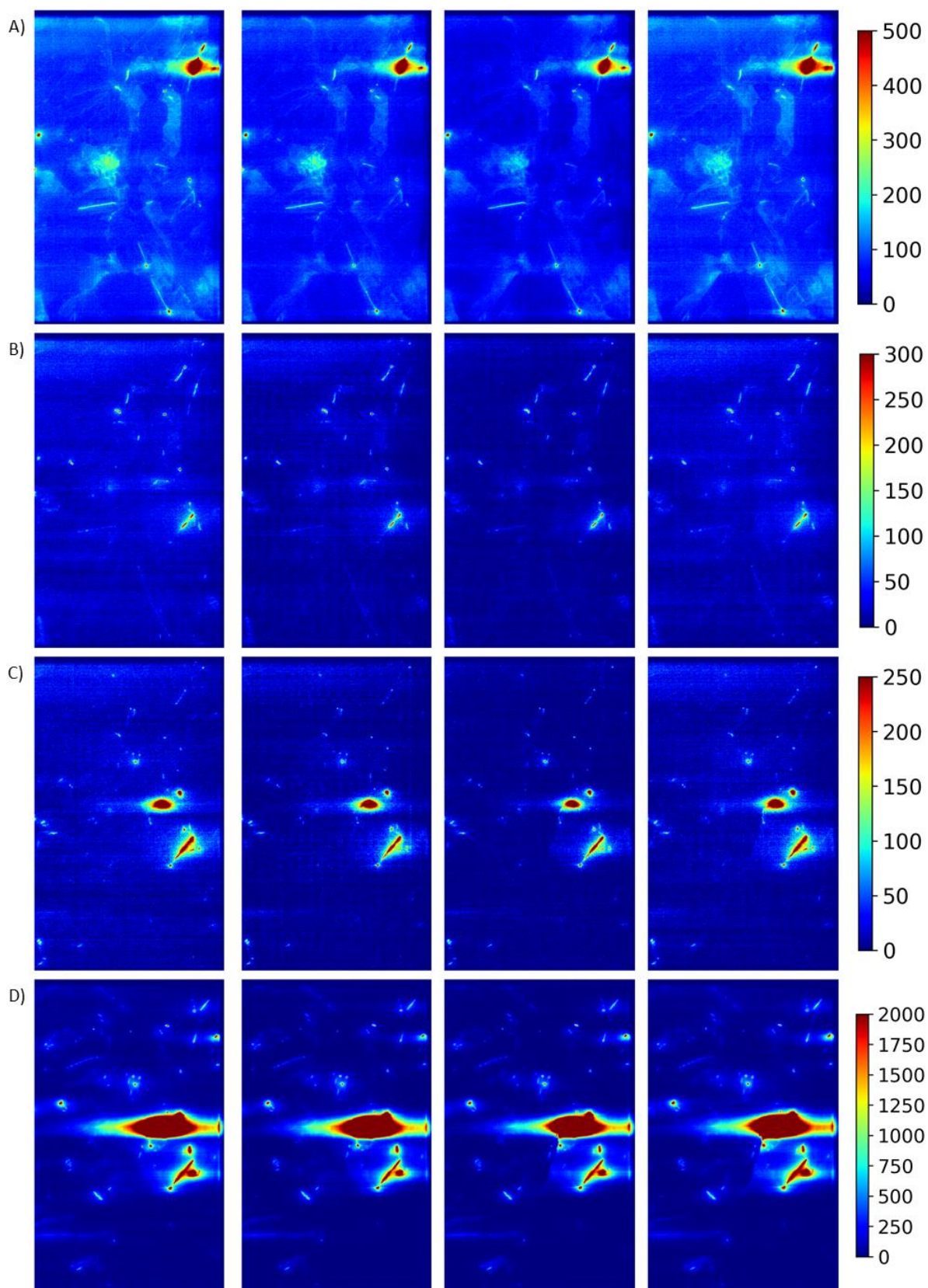


Figure 4.17: Sample S2 CL: Surface passivated, phosphorus diffusion gettering treated and hydrogen bulk passivated, lower half of sample. Images at different photon energies (A – D) and after different processing times (left to right). The processing times are, from left to right, initial (0), 84 hours of light soaking, 60 and 1020 minutes of light and heat treatment. A) D3 signal. B) D2 signal. C) D1 signal. D) D07 signal. Some of the images are processed to have high saturation (the big, dark red spots) to emphasise the spots and regions with lower signal intensity.



## Results and Discussion

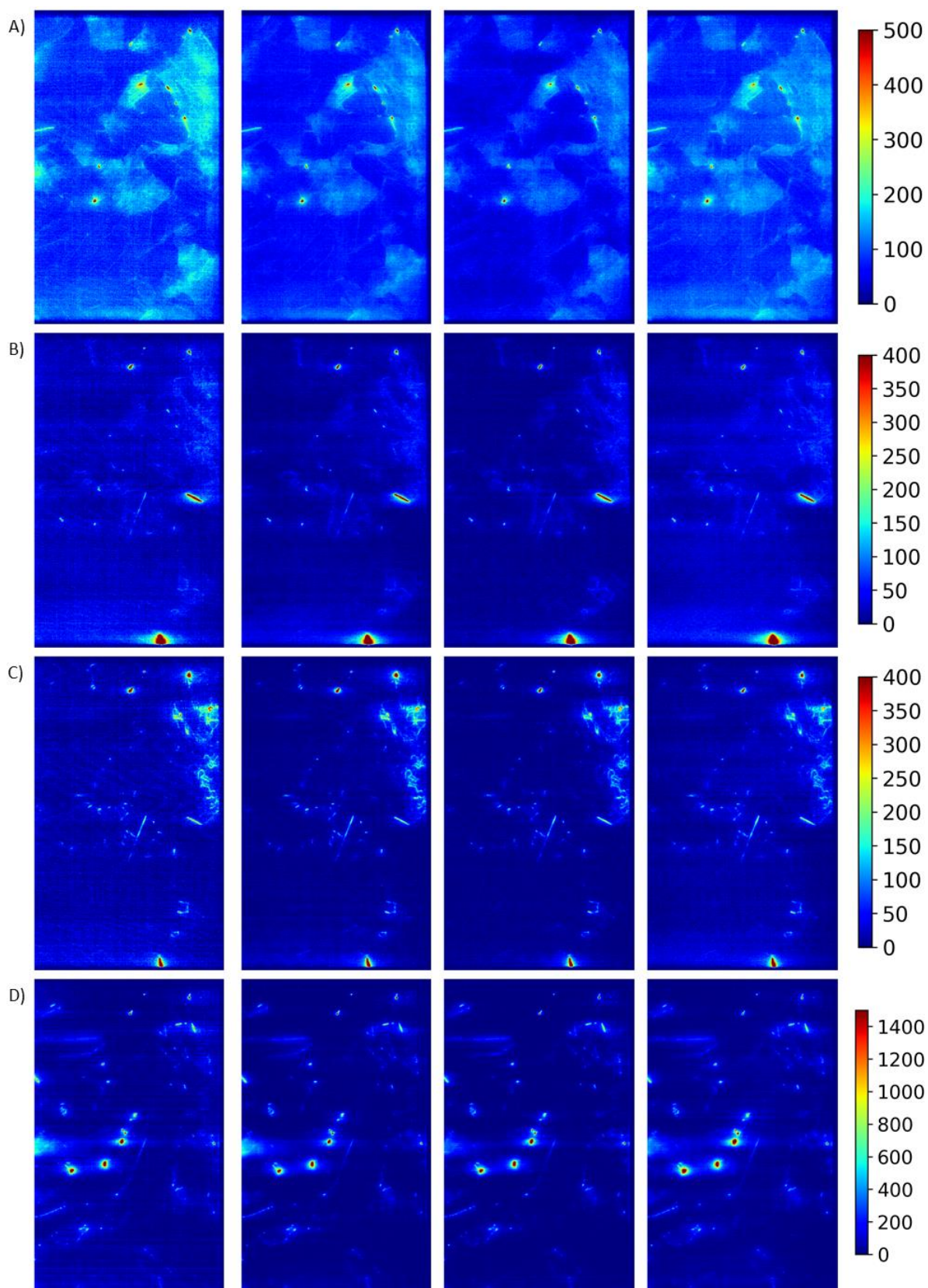


Figure 4.18: Sample S2 CU: Surface passivated, phosphorus diffusion gettering treated and hydrogen bulk passivated, upper half of sample. Images at different photon energies (A – D) and after different processing times (left to right). The processing times are, from left to right, initial (0), 84 hours of light soaking, 60 and 1080 minutes of light and heat treatment. A) D3 signal. B) D2 signal. C) D1 signal. D) D07 signal. Some of the images are processed to have high saturation (the big, dark red spots) to emphasise the spots and regions with lower signal intensity.

## Results and Discussion

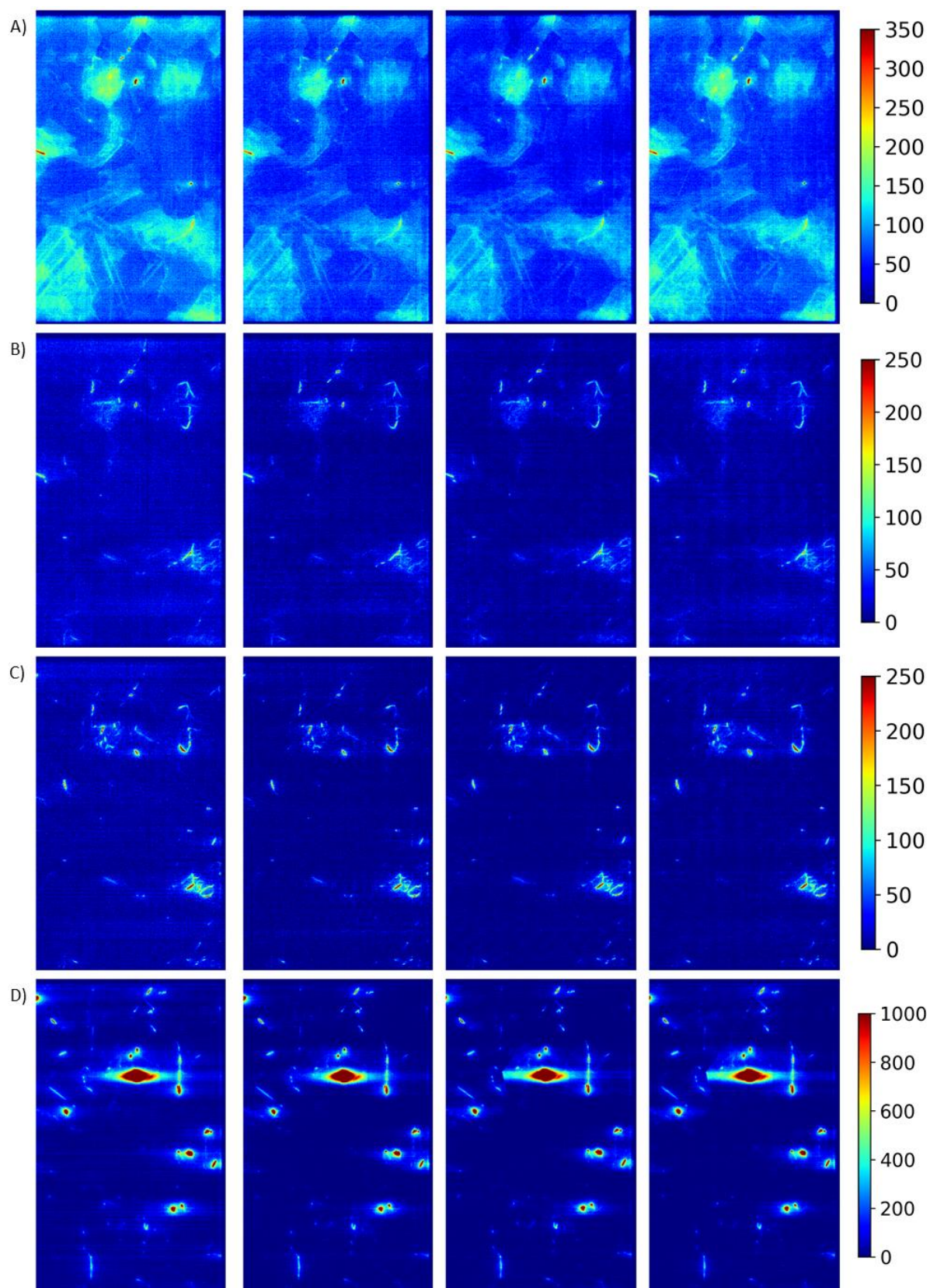


Figure 4.19: Sample S2 DL: Surface passivated, phosphorus diffusion gettering treated and hydrogen bulk passivated, lower half of sample. Images at different photon energies (A – D) and after different processing times (left to right). The processing times are, from left to right, initial (0), 84 hours of light soaking, 60 and 1020 minutes of light and heat treatment. A) D3 signal. B) D2 signal. C) D1 signal. D) D07 signal. Some of the images are processed to have high saturation (the big, dark red spots) to emphasise the spots and regions with lower signal intensity.

## Results and Discussion

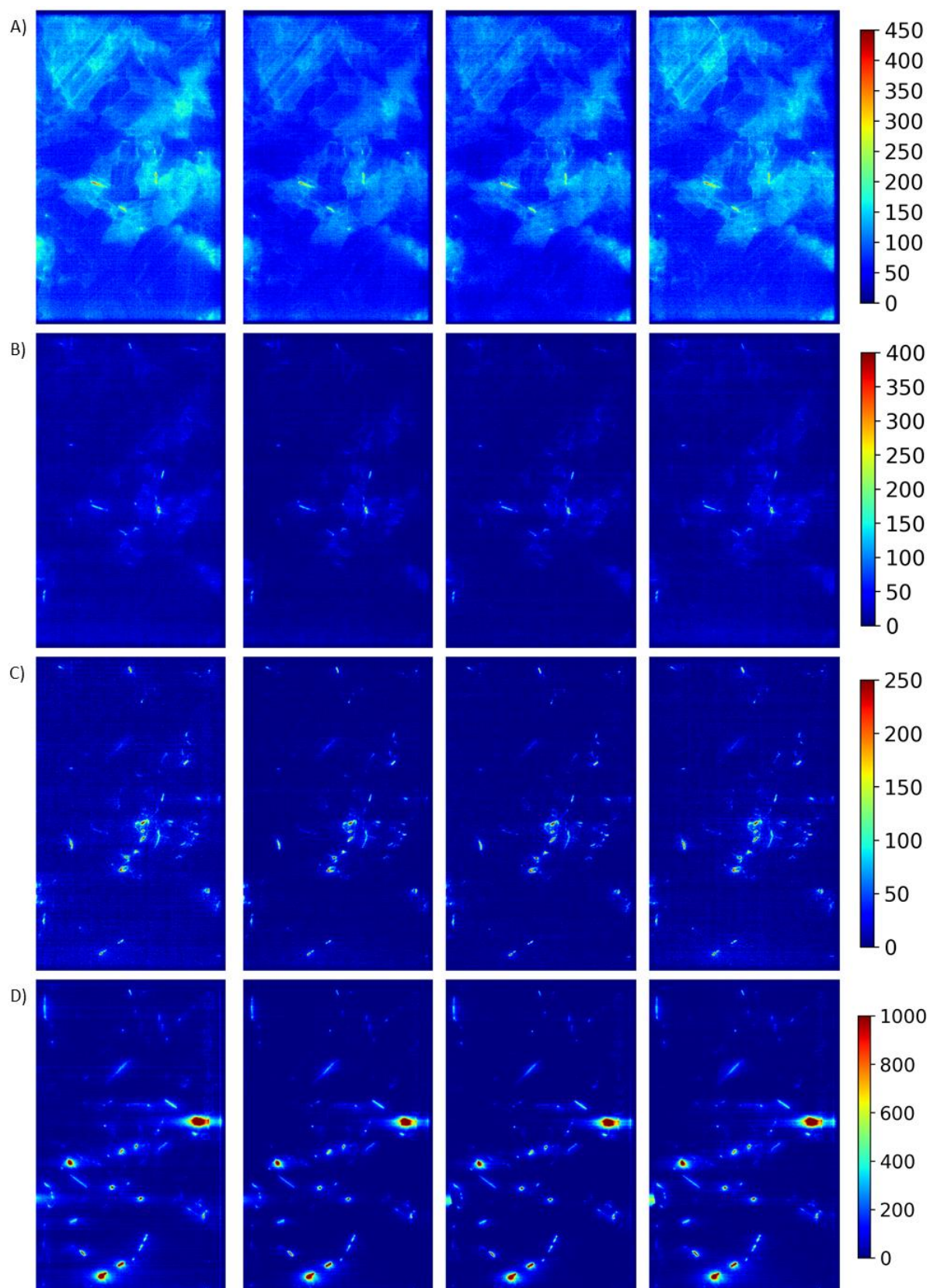


Figure 4.20: Sample S2 DU: Surface passivated, phosphorus diffusion gettering treated and hydrogen bulk passivated, upper half of sample. Images at different photon energies (A – D) and after different processing times (left to right). The processing times are, from left to right, initial (0), 84 hours of light soaking, 120 and 1080 minutes of light and heat treatment. A) D3 signal. B) D2 signal. C) D1 signal. D) D07 signal. Some of the images are processed to have high saturation (the big, dark red spots) to emphasise the spots and regions with lower signal intensity.

## Results and Discussion

The DRL signals seem to follow the same trend of degradation and recovery as the BB signal. This was unexpected as one should expect the DRL signals, the signals of reduced lifetime, to follow the opposite trend of the BB signal, the signal of high lifetime. But this is not the case.

The DRL signals share many of the same spatial points and regions and occupy the opposite regions of where the BB signal is strong. This is not surprising as impurities and defects tend to coincide. That the DRL signal (of low lifetime) occupy the opposite regions of where the BB signal (of long lifetime) is high is also as expected. The samples are of the high performance multicrystalline variant, involving that the crystals are kept relatively small to increase performance by allowing impurities to diffuse to surrounding crystal edges and concentrate there, rather than reducing the effectiveness of the bulk of the wafer. This effect is seen here, as the impurity signals (DRL) does not occupy region/points in the high BB signal regions but stick to the high DRL regions. The anti-correlation of the BB signal and the DRL is clearest when looking at the D3 signal, which share the regional nature of the BB signal.

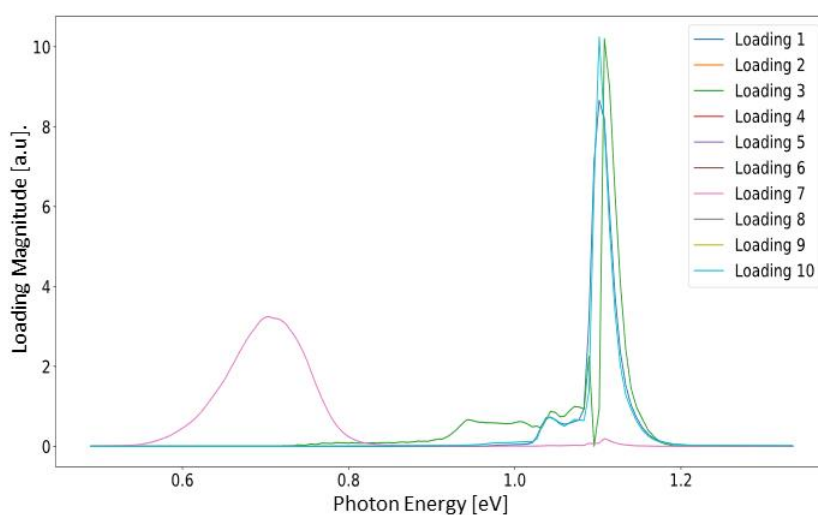
That DRL signal does not appear or disappear should also be noted. One of the questions concerning LeTID was whenever the reduced performance was caused by some new defect appearing. This seems not to be the case, at least not for the examined DRL signals of D3, D2, D1 and D07. On this note a further search for other DRL signals was performed in the form of an MCR analysis in the next section.

#### 4.4 MULTIVARIATE CURVE RESOLUTION ANALYSIS

In a search for other DRL signals that may be related to LeTID an MCR analysis was performed. Figure 4.21 shows the result an MCR analysis computed with 10 components for the sample S2 CL in the initial state. Only 4 loadings and scores are shown in the figures as the other components yielded all-zero results. Other numbers of components and in other states of processing were also tested but yielded similar results and are therefore not included.

Component 1 (seen as Loading 1 in A) and score 1 in B)) captures parts of the BB signal around 1.1 eV together with a signal at about 1.03 eV. Component 3 captures another part of the BB signal as well as signals in the 0.93 to 1.1 eV range. Component 7 captures a signal with a peak at 0.7 eV, shown mostly as a single strong point in the B) subfigure. Loading 10 very much mirrors loading 1 but partly occupy different regions in the score plot. Component 1, 3 and 10 all occupy broad regions in the score plot, rather than strong points or lines.

A)



B)

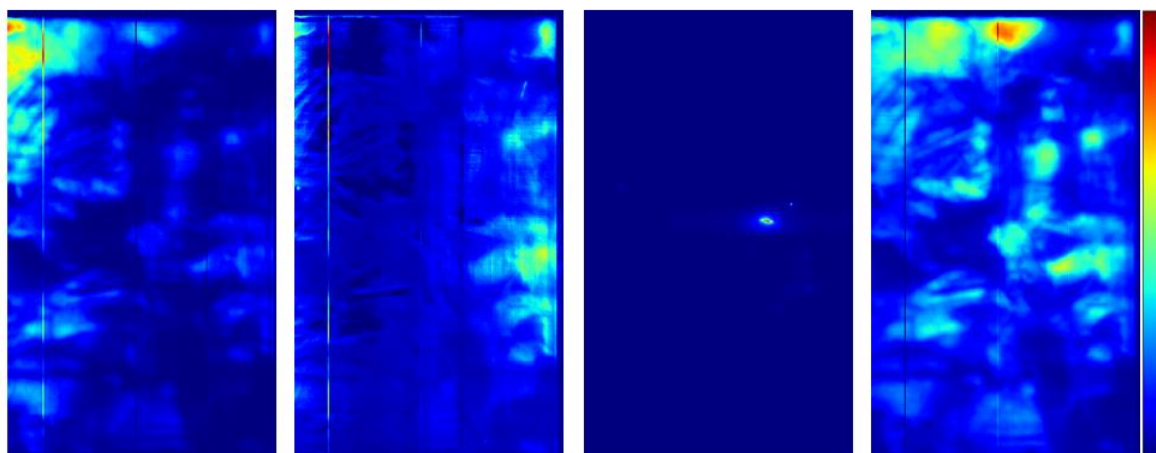


Figure 4.21: Multivariate Curve Resolution Analysis (MCR) of sample S2 CL (Surface passivated, phosphorus diffusion gettering treated and hydrogen bulk passivated, lower half of sample) in the initial state (no heat or light treatment). 10 components have been calculated, but only 4 loadings (A) and 4 scores (B) are displayed as the rest were all-zero. A) Loading magnitude plotted versus photon energy. B) Score plots, from left to right: Score 1, score 3, score 7 and score 10.

## Results and Discussion

Component 1 captures the BB signal and what is assumed to be a phonon replica of the BB signal, given its photon energy and spatial expanse in the same regions as the BB signal. The BB signal dominates the Score 3 plot, while the signal peaks in the 0.93-1.1 eV range of the loadings plot coincide with the D3 and D4 signals together with phonon replicas. Loading 7 has its peak at 0.7 eV and the score 7 plot is dominated by a strong point signal, suggesting this signal to be D07. The score 7 plot's point also occupies the same position as the point in the D07 spatial plot. The broad loading 7 peak might be deconvoluted into different DRL signals, with the same spatial origin, but I have not found this to be the case. Component 10 captures the same BB and BB phonon replica type signals as component 1, just occupying different spatial regions. Component 1, 3 and 10 all occupying broad regions in the score plot, rather than strong points or lines, supports them being BB signals as the BB signal shares this trait.

The MCR analysis thus could not find any DRL signals apart from the already known D4, D3 and D07 signals.

### 4.5 ROUNDING OF DISCUSSION

The LeTID effect is only seen in the surface passivated PDGH samples. Both a high hydrogen concentration and high charge carrier density seem to be prerequisites for the LeTID to occur, as LeTID does not occur without both hydrogen bulk passivation (PDGH processing causing high hydrogen concentration) and surface passivation (with causes significantly increased charge carrier density<sup>11</sup>). A hydrogen effect is one of the suspected mechanisms to cause LeTID in the LETuP project<sup>6</sup>, as suggested in previous research<sup>9,10</sup>.

For all samples a LID effect is observed. It is observed as a recovery by light and heat processing for the samples in set 1, and both a degradation with light soaking and a recovery with light and heat processing for the samples in set 2. In both cases Boron-Oxygen related LID seems to be the cause when compared to previous research<sup>20,21</sup>.

Both the LID and LeTID primarily occur in regions on the samples where the BB signal is moderate and high, suggesting that the material need to be sufficiently defect free and pure for there to be a BB signal to degrade. The DRL signals occupy the opposite regions. They decrease and increase following the same pattern as the BB signal do, and not the opposite pattern one might expect. These DRL signals does not disappear when they are degraded, only decreases their intensity. Nor does new DRL signals appear as the BB signal is reduced. The DRL signals observed are the D4, D3, D2, D1, VID3 and D07. Other signals are not found with an MCR analysis either.

Challenges met during the experimental work for this thesis included the accumulation of frozen dew on the sample holder between imaging and on the samples during imaging. The frost protection screening used is not enough. Dew was removed before each session of imaging, as well as at regular intervals between imaging of the different samples. The dew was not removed between each sample but done often enough to be deemed satisfactory. Further work with the imaging setup, after the data collection for this thesis, has shown that even small amount of dew can disturb a consistent imaging of the samples. More images were to be taken with a hopefully improved setup but were cancelled due to time constraint.

The dew problem was made worse by the way the camera disconnection from the computer used to control the setup and collect the data. This happened when static shocks struck the closet as we opened the doors for sample handling. This caused the control program to need a restart, leaving time for dew to collect on the sample holder. This dew was removed before imaging, but still causes an inconsistency in the dew removal routine.

Samples were usually imaged right away as they were removed for the light (and heat) processing. This was not always the case thou, as this was not thought to be affecting the samples nor the imaging of them. In one instance samples waited up to about 1.5 hours before imaging after

## Results and Discussion

processing. At some point during the experiment this was investigated, and it turned out that at least the BB signal was affected by the waiting. This can be seen for points in the A) figures of Figures 4.1 - 4.16 as points with the same processing time, but different signal magnitude. Even when the routine was more consistent, the last image of each session was taken at least 18 minutes after the first image.

A lot of data is collected from the imaging setup. To find the right way of analysing and visualising this data is no trivial task. Known photon energies of significance was of great help together with MCR analysis to find other signal, but no guarantee for all the possible discoveries to be uncovered form amongst the less significant signals and noise.









## 5 CONCLUSION

High performance multicrystalline silicon wafers of different processing have been investigated using a hyperspectral photoluminescence imaging setup for light and elevated temperature induced degradation and its effect on the band-to-band and defect related luminescence signals, which are associated with good and poor solar cell performance respectively. The wafers samples have been with removed and intact surface passivation, and of three different degrees of treatment with respect to gettering and bulk hydrogenation passivation. The imaging has been done at 90 K in between light soaking at 0.23 suns and light and heat processing at 0.79 suns and 150 °C.

For the LeTID to be observed the samples must be both surface passivated, phosphorus diffusion gettering processed and bulk passivated with hydrogen. This is presented in Table 5.1, which is a completed version of Table 1.1 from the introduction. That the samples must be surface passivated suggests that a high charge carrier concentration is a prerequisite for LeTID to occur. That the samples must be bulk passivated with hydrogen suggest that a hydrogen effect is the mechanism that causes LeTID.

*Table 5.1: LeTID is only observed in the surface passivated PDGH samples (Phosphorus diffusion gettering processed and bulk passivated using hydrogen). That the samples must be PDGH processed suggests that a hydrogen effect is causing LeTID, and this only occur with high charge carrier density for which surface passivation is needed.*

	Surface Passivation Removed	Surface Passivated
As cut		
PDG		
PDGH		

LeTID is seen to affect both the BB signal and the DRL signals. The BB signal degrades and is recovered when exposed to light and elevated temperatures, as is the case for lifetime measurements in previous LeTID studies<sup>27</sup>. A surprise is that the DRL signals (D3, D2, D1 and D07) follow the same trend of degradation and recovery as the BB signal does. The DRL signals observed does not disappear or appear as a result of LeTID, only changing intensity. That is, no new defects or impurities seem to appear or be activated, rather LeTID affects the activeness of the already present defects.

For further work on the set up, or a similar one, better management of frozen dew and air humidity should be a priority. A better device for keeping hot air away from the sample holder and cooled samples could be designed. Even better would be to further reduce the air humidity in the room. A better way to reduce static electricity interfering with the electronics should also be considered as interruptions disturb the measurement and frost removal routine. Further study of the

## Conclusion

effect of waiting between processing and imaging might be of interest. At the least a more rigorous routine for imaging at a set time after processing should be incorporated. This problem is however reduced if interruptions due to static shocks and dew removal are reduced by the above-mentioned suggestions. A reference wafer could be included within the frame of the images to calibrate the images against, making it easier to compare images from different sessions.

The insight gained from this study contributes to the broader study of LeTID and the improvement of PV technology. Especially the observation that PDGH treatment and surface passivation is needed for LeTID to occur might contribute to the work to improve the solar cells of tomorrow.

## 6 REFERENCES

1. Shafiee, S. & Topal, E. (2009). When will fossil fuel reserves be diminished? *Energy Policy*, 37 (1): 181-189. doi: 10.1016/j.enpol.2008.08.016.
2. IPCC. (2014). *Climate Change 2014: Impacts, Adaptation, and Vulnerability*. Part A: Global and Sectoral Aspects. Contribution of Working Group II to the Fifth Assessment Report of the Intergovernmental Panel on Climate Change. New York, NY, USA: IPCC.
3. IPCC. (2014). *Climate Change 2014: Mitigation of Climate Change*. Contribution of Working Group III to the Fifth Assessment Report of the Intergovernmental Panel on Climate Change. New York, NY, USA: IPCC.
4. ITRPV. (2019). *2018 Results*. 10th Edition: International Technology Roadmap for Photovoltaics (ITRPV).
5. NREL. (2017). *Best Research-Cell Efficiencies*. Golden, Colorado: United States Department of Energy.
6. LETuP. (2018). *LeTID in multicrystalline PERC cells*. Unpublished manuscript.
7. Flø, A. (2014). *Hyperspectral Imaging as a Tool for Characterization of Multicrystalline Silicon Wafers*. Philosophiae Doctor (PhD) Thesis. Ås: Norwegian University of Life Sciences.
8. Burud, I., Mehl, T., Flo, A., Lausch, D. & Olsen, E. (2016). Hyperspectral photoluminescence imaging of defects in solar cells. *Journal of Spectral Imaging*, 5 (a8). doi: 10.1255/jsi.2016.a8.
9. Eberle, R., Kwopil, W., Schindler, F., Schubert, M. & Glunz, S. (2016). Impact of the firing temperature profile on light induced degradation of multicrystalline silicon. *physica status solidi (RRL) – Rapid Research Letters*: n/a-n/a. doi: 10.1002/pssr.201600272.
10. Chan, C., Fung, T. H., Abbott, M., Payne, D., Wenham, A., Hallam, B., Chen, R. & Wenham, S. (2017). Modulation of Carrier-Induced Defect Kinetics in Multi-Crystalline Silicon PERC Cells Through Dark Annealing. *Rapid Research Letter*, 1 (2): 1600028. doi: 10.1002/solr.201600028.
11. Smets, A., Jäger, K., Isabella, O., Swaaij, R. & Zeman, M. (2016). *Solar Energy: The Physics and Engineering of Photovoltaic Conversion Technologies and Systems*. Cambridge: UIT Cambridge Ltd.
12. Hull, R. (1999). *Properties of Crystalline Silicon*. London, United Kingdom: INSPEC, The Institution of Electrical Engineers.
13. Drozdov, N., Patrin, A. & Tkachev, V. (1976). Recombination radiation on dislocations in silicon. *Jetp Letters*, 23 (11): 597-599.
14. Flø, A., Burud, I., Kvaal, K., Søndena, R. & Olsen, E. (2013). Distribution of radiative crystal imperfections through a silicon ingot. *AIP Advances*, 3 (112120). doi: 10.1063/1.4834155.
15. Pizzini, S., Grilli, E., Guzzi, M. & Borionetti, G. (2000). Photoluminescence emission in the 0.7-0.9 eV range from oxygen precipitates, thermal donors and dislocations in silicon. *Journal of Physics: Condensed Matter*, 12 (49). doi: 10.1088/0953-8984/12/49/312.
16. Mehl, T. (2018). *Hyperspectral Photoluminescence Imaging of Silicon Wafers and Solar Cells*. Philosophiae Doctor (PhD) Thesis. Ås: Norwegian University of Life Sciences.
17. Ashcroft, N. W. & Mermin, N. D. (1976). *Solid state physics*. New York: Holt, Rinehart and Winston.
18. Viña, L., Logothetidis, S. & Cardona, M. (1984). Temperature dependence of the dielectric function of germanium. *Physical Review B*, 30 (4). doi: 10.1103/PhysRevB.30.1979.
19. Petter, K. et al. (2016). *Dependence of LeTID on brick height for different wafer suppliers with several resistivities and dopants*. The 9th Int. Work. Cryst. Si Solar Cells.
20. Nærland, T., Haug, H., Angelskår, H., Søndena, R., Marstein, E. & Arnberg, L. (2013). Studying Light-Induced Degradation by Lifetime Decay Analysis: Excellent Fit to Solution of Simple Second-Order Rate Equation. *IEEE Journal of Photovoltaics*, 3: 1265-1270. doi: 10.1109/JPHOTOV.2013.2278663.
21. Søndena, R. & Ghaderi, A. (2014). *Quantification of LID in Multicrystalline Silicon Wafers*. 29th European Photovoltaic Solar Energy Conference and Exhibition, Amsterdam, Netherlands.

## References

22. Ramspeck, K., Zimmermann, S., Nagel, H., Metz, A., Gassenbauer, Y., Birkmann, B. & Seidl, A. (2012). *Light induced degradation of rear passivated mc-Si solar cells*. 27th European Photovoltaic Solar Energy Conference and Exhibition.
23. Bredemeier, D., Walter, D., Herlufsen, S. & Schmidt, J. (2016). Lifetime degradation and regeneration in multicrystalline silicon under illumination at elevated temperature. *AIP Advances*, 6(3):035119. doi: 10.1063/1.4944839.
24. Mehl, T., Wyller, G. M., Burud, I. & Olsen, E. (2019). Increased sensitivity in near infrared hyperspectral imaging by enhanced background noise subtraction. *Journal of Spectral Imaging*, 8. doi: 10.1255/jsi.2019.a2.
25. Ruckebusch, C. & Blanchet, L. (2013). Multivariate curve resolution: A review of advanced and tailored applications and challenges. *Analytica Chimica Acta*, 765: 28-36. doi: 10.1016/j.aca.2012.12.028.
26. Burud, I., Flø, A. & Olsen, E. (2012). On the origin of inter band gap radiative emission in crystalline silicon. *AIP Advances*, 2 (042135). doi: 10.1063/1.4766588.
27. Søndena, R. (2018). *Samples for spectral-PL 2019*. Unpublished manuscript.

## APPENDICES

---

### A) PYTHON FUNCTION FOR READING HSPL IMAGES INTO MEMORY

A function that reads all the images of one sample into memory, cropping the parts of the images that do not include the sample. The images should be stored in a folder with a subfolder for each image (where each image consist of three images that are combined as a median of the three). Each image represents the sample at a given state of processing. It uses functions for data pre-processing, including background correction, written by Marija Vukovic.

```

1. # -*- coding: utf-8 -*-
2.
3. import sys
4. sys.path.append('C://Dropbox/NMBU_Siv.Ing/MASTER/Kode_Python/PythonPackages/')
5.
6. import os
7. import numpy as np
8. from General import ReadImages, ExtractFrame
9. from CorrectionOldCamera import MedianHyperspectral
10.
11.
12. def read_crop_images_from_folders(superfolder, sample=None, crop=None):
13.     """
14.     Function to read and crop images from a folder.
15.     The folder(superfolder) should have a subfolder for each median image that
16.     is to be made, containing the .raw and .hdr files for three - 3 - images.
17.     Parameters
18.     -----
19.     superfolder : string
20.         A string with the directory of the folder containing the images
21.     sample : dictionary
22.         A dictionary that is to be extended with the images in the given superfolder
23.         If None, a dictionary will be created.
24.     crop : None, 'auto', or a tuple (xleft,xright,ytop,ybottom)
25.         Argument to describe the desired cropping of the median image.
26.         None will leave the median image uncropped.
27.         'auto' will use the ExtractFrame-
28.         module to automatically crop the median image.
29.         A tuple of 4 integers will crop the median image as defined by the
30.         four cornes in the tuple: (xleft,xright,ytop,ybottom)
31.     Returns
32.     -----
33.     sample : dictionary
34.         A dictionary with the median images in the folder superfolder.
35.     """
36.
37.     old_folder = os.getcwd()
38.     os.chdir(superfolder)
39.
40.     if sample is None:
41.         sample = {}
42.
43.     for folder in os.listdir():
44.         print(folder) # Nice to keep track of progress
45.         os.chdir(superfolder+'/'+folder)
46.         img = ReadImages.read_images_from_folder('*.raw')
47.

```

## Appendices

```
48.     # If median is not made (due to different matrix length),
49.     # the last lines are cropped and median is made.
50.     if img.shape == (3,):
51.         length = min(img[0].shape[0],
52.                       img[1].shape[0],
53.                       img[2].shape[0])
54.         img[0] = img[0][:length, :, :]
55.         img[1] = img[1][:length, :, :]
56.         img[2] = img[2][:length, :, :]
57.         img = MedianHyperspectral.make_median_img(img[0], img[1], img[2])
58.
59.     # Cropping of non Silicon pixels
60.     np.nan_to_num(img, False) # NaN disturbs the auto cropping
61.     if crop == 'auto':
62.         classes = ExtractFrame.k_means(img, 6, 10)
63.         sample['{}'.format(folder)] = \
64.             ExtractFrame.extract_frame(classes, img, max_upper_rows=True,
65.                                       max_lower_rows=True,
66.                                       max_left_columns=True,
67.                                       max_right_columns=True)
68.
69.     elif type(crop) == tuple:
70.         sample['{}'.format(folder)] = img[crop[2]:crop[3], crop[0]:crop[1], :]
71.
72.     else:
73.         sample['{}'.format(folder)] = img
74.
75.     os.chdir(old_folder)
76.     return sample
```

## B) PYTHON FUNCTION FOR SORTING THE IMAGES BY PROCESSING TIME

A function to sort the images in a dictionary as returned by the function in Section A). The images are sorted so the light soaked images come before the light and heat processes images. Mehl20190131 and Mehl20190204, and Mehl20190116, are the datasets used for this thesis.

```

1. # -*- coding: utf-8 -*-
2.
3. import numpy as np
4. import natsort
5. import os
6.
7.
8. def sort_images_keys(images, output='0hm'):
9.     """
10.    Function that sorts images.
11.    Made with Mehl20190131 and Mehl20190204 data in mind:
12.    AU0
13.    AU10m
14.    ...
15.    AU16h
16.    0 comes first, then m, then h.
17.
18.    Parameters
19.    -----
20.    images : dictionary
21.        A dictionary with the images (e.g. from one sample over time, as made by
22.        General.ReadFolders.read_crop_images_from_folders).
23.    output : string
24.        A string to determine which list to be returned:
25.        '0' - Return the images ending with '0'
26.        'h' - Return the images ending with 'h'
27.        'm' - Return the images ending with 'm'
28.        It may be a combination, e.g. '0h' will return both 0 and h images
29.
30.    Returns
31.    -----
32.    keys : list
33.        A sorted list with the keys from the dictionary 'images'.
34.    """
35.
36.    keys = list(images.keys())
37.    zero = []
38.    hours = []
39.    minutes = []
40.    for key in keys:
41.        if key[-1] == '0':
42.            zero.append(key)
43.        elif key[-1] == 'h':
44.            hours.append(key)
45.        else:
46.            minutes.append(key)
47.
48.    keys = [] # A whole new keys-list. This will be returned
49.    if '0' in output:
50.        keys += natsort.humansorted(zero)
51.    if 'h' in output:
52.        keys += natsort.humansorted(hours)
53.    if 'm' in output:
54.        keys += natsort.humansorted(minutes)
55.
56.    return keys

```

## C) PYTHON FUNCTIONS FOR PLOTTING DEVELOPMENT IN THE SAMPLE-WIDE BB SIGNAL

Functions for plotting the development in the sample-wide BB signal as described in Section 3.3.2 and seen in the A) figures of Figures 4.1 - 4.16. `imgPLdev` and `imgPLdev16` are almost identical but designed for working with slightly differently organised images. `imgSpectrum` is presented in Section D).

```

1. # -*- coding: utf-8 -*-
2.
3. import sys
4. sys.path.append('C://Dropbox/NMBU_Siv.Ing/MASTER/Kode_Python/PythonPackages/')
5.
6. import numpy as np
7. import matplotlib.pyplot as plt
8. from General.ImgTransision import sort_images_keys
9.
10. from scipy.io import loadmat
11. eV = loadmat('C://Dropbox/NMBU_Siv.Ing/MASTER/Kode_Python/PythonPackages/FunctionsFor
    MCR/Energi_specimOct2014.mat')['Ev'] # Vector with the electronvolt values
12.
13. transisions = {'BB' : np.arange(29, 34),
14.               'D4' : np.arange(47, 52),
15.               'D3' : np.arange(58, 64),
16.               'D2' : np.arange(76, 82),
17.               'D1' : np.arange(92, 99),
18.               'D07': np.arange(115, 143),
19.               'DRL': np.arange(45, 200)}
20.
21.
22. def imgPLdev(images, title, transision, LeT=False,
23.             ylabel='Relative PL Intensity', xlabel='Processing Time',
24.             ref=None, save=False,
25.             curfig=None, curax=None):
26.
27.     """
28.     Function to plot the development in a PL signal for a (cropped) set of
29.     images as function of processing time.
30.     The signal in summed over the image (x,y,wavelength) for given wavelength-
    bands (transision).
31.     The images are from one sample, in a dictionary.
32.     Should be used with function imgPLdev_dual.
33.     Designed for dataset Mehl 20190131+20190204
34.     """
35.     if LeT:
36.         keys = sort_images_keys(images, output='m')
37.         style = 'ro'
38.     else:
39.         keys = sort_images_keys(images, output='0h')
40.         style = 'bo'
41.
42.     if curfig is None:
43.         fig, ax = plt.subplots()
44.     else:
45.         fig, ax = curfig, curax
46.
47.     # Get points to plot, and the referance for the y-axis.
48.     signals = np.zeros(len(keys))
49.     times = np.zeros(len(keys))
50.     for i, key in enumerate(keys):
51.         signals[i] = np.sum(imgSpectrum(images[key])[transisions[transision]])
52.
53.     if LeT:
54.         time = int(key[2:-1])

```



```

55.         else:
56.             time = key[2:-1]
57.             if time == '':
58.                 time = int(0)
59.             else:
60.                 time = int(time)
61.             times[i] = time
62.
63.         # Calculate reference if it is not given as input
64.         if ref is None:
65.             ref = np.mean(signals)
66.         signals /= ref
67.
68.         ax.plot(times, signals, style)
69.         ax.set(title='', ylabel=ylabel, xlabel=xlabel)
70.
71.         if save:
72.             plt.savefig(title+'.svg')
73.         return ax, ref
74.
75.
76. def imgPLdev16(images, title, transision,
77.               ylabel='Relative PL Intensity', xlabel='Processing Time [min]',
78.               ref=None, save=False,
79.               curfig=None, curax=None):
80.
81.     """
82.     Function to plot the development in a PL signal for a (cropped) set of
83.     images as function of processing time.
84.     The signal is summed over the image (x,y,wavelength) for given wavelength-
85.     bands (transision).
86.     The images are from one sample, in a dictionary.
87.     Designed for dataset Mehl 20190116
88.     """
89.     style = 'ro'
90.     keys = sort_images_keys(images)
91.
92.     if curfig is None:
93.         fig, ax = plt.subplots()
94.     else:
95.         fig, ax = curfig, curax
96.
97.     # Get points to plot, and the reference for the y-axis.
98.     signals = np.zeros(len(keys))
99.     times = np.zeros(len(keys))
100.    for i, key in enumerate(keys):
101.        signals[i] = np.sum(imgSpectrum(images[key])[transisions[transision]]
102.    )
103.        time = int(key[2:])
104.
105.        times[i] = time
106.
107.    # Calculate reference if it is not given as input
108.    if ref is None:
109.        ref = np.mean(signals)
110.    signals /= ref
111.
112.    ax.plot(times, signals, style)
113.    ax.set(title='', ylabel=ylabel, xlabel=xlabel)
114.
115.    if save:
116.        plt.savefig(title+'.svg')
117.    return ax, ref
118.

```

## Appendices

```
119.
120.     def imgPLdev_dual(images, title, transision,
121.                       ylabel='Relative PL Intensity',
122.                       xlabel1='Processing Time [h]',
123.                       xlabel2='Processing Time [min]',
124.                       ref=None,
125.                       save=False):
126.         """
127.         Function to plot two windows of the development in a PL signal for a (cro
128.         pped)
129.         set of images as function of processing time.
130.         See the function imgPLdev.
131.         Default reference is the mean of the points in the non-LeT window
132.         """
133.
134.         fig = plt.figure()
135.         fig.add_axes()
136.         ax1 = fig.add_subplot(121)
137.         ax2 = fig.add_subplot(122, sharey=ax1)
138.
139.         ax1, ref1 = imgPLdev(images, title='', transision=transision, LeT=False,
140.                              ylabel=ylabel,
141.                              xlabel=xlabel1,
142.                              save=False,
143.                              curfig=fig,
144.                              curax=ax1,
145.                              ref=ref)
146.
147.         ax2, ref2 = imgPLdev(images, title='', transision=transision, LeT=True,
148.                              ylabel='',
149.                              xlabel=xlabel2,
150.                              save=False,
151.                              curfig=fig,
152.                              curax=ax2,
153.                              ref=ref1)
154.
155.         fig.suptitle('')
156.
157.         if save:
158.             plt.savefig(title+'.svg')
159.         return fig, ax1, ax2
```

## D) PYTHON FUNCTIONS FOR PLOTTING DEVELOPMENT OF THE DIFFERENT PHOTON ENERGIES

Functions for plotting the development in the sample-wide photon energies as described in Section 3.3.2 and seen in the B) figures of Figures 4.1 - 4.16. `imgSpectrumDev` and `imgSpectrumDev16` are almost identical but designed for working with slightly differently organised images.

```

1. # -*- coding: utf-8 -*-
2.
3. import sys
4. sys.path.append('C://Dropbox/NMBU_Siv.Ing/MASTER/Kode_Python/PythonPackages/')
5.
6. import numpy as np
7. import matplotlib.pyplot as plt
8. from General.ImgTransion import sort_images_keys
9.
10. from scipy.io import loadmat
11. eV = loadmat('C://Dropbox/NMBU_Siv.Ing/MASTER/Kode_Python/PythonPackages/FunctionsFor
    MCR/Energi_specimOct2014.mat')['Ev']
12.
13.
14. def imgSpectrum(image):
15.     """Function to make Spectrum-vector of an image"""
16.     spec = np.sum(np.sum(image, axis=0), axis=0)
17.     return spec - np.nanmin(spec)    # Adjust for noise and zero level
18.
19.
20. def imgSpectrumNormalized(image):
21.     """Function to make Spectrum-vector of an image, with normalization"""
22.     spec = np.sum(np.sum(image, axis=0), axis=0)
23.     spec -= np.nanmin(spec)    # Adjust for noise and zero level
24.     x = image.shape[0]
25.     y = image.shape[1]
26.     return spec/(x*y)    # Divide by size of image
27.
28.
29. def imgSpectrumDev(images, title, ylabel='PL Intensity [a.u]',
30.                    xlabel='Photon Energy [eV]',
31.                    normalize=False, save=False):
32.     """Function to plot Spectrum of a sample over time"""
33.
34.     # dicts to convert from name to color and linewidth
35.     name2color = {'0' : 'k',
36.                  '16h' : 'y',
37.                  ...
38.                  '1322m': 'orange',
39.                  '1323m': 'm'}
40.
41.     name2width = {'0' : 1,
42.                  '16h' : 1,
43.                  ...
44.                  '1322m': 3,
45.                  '1323m': 4}
46.
47.     keys = sort_images_keys(images)
48.
49.     fig, ax = plt.subplots()
50.     for key in keys:
51.         if normalize:
52.             spectrum = imgSpectrumNormalized(images[key])
53.         else:
54.             spectrum = imgSpectrum(images[key])
55.         lines = ax.plot(eV, spectrum, label=key,

```

## Appendices

```
56.             color=name2color[key[2:]],
57.             linewidth=name2width[key[2:]])
58.
59.     ax.set(title='', ylabel=ylabel, xlabel=xlabel)
60.     ax.legend(loc='best')
61.
62.     if save:
63.         plt.savefig(title+'.svg')
64.
65.
66. def imgSpectrumDev16(images, title, ylabel='PL Intensity [a.u]',
67.                    xlabel='Photon Energy [eV]',
68.                    normalize=False, save=False):
69.     """
70.     Function to plot Spectrum of a sample over time
71.     Made for Mehl20190116
72.     """
73.
74.     # dicts to convert from name to color and linewidth
75.     name2color = {'0' : 'k',
76.                  '10' : 'r',
77.                  '20' : 'r',
78.                  '30' : 'r',
79.                  '60' : 'r',
80.                  '120' : 'r',
81.                  '300' : 'g',
82.                  '1020' : 'g',
83.                  '1021' : 'g'}
84.
85.     name2width = {'0' : '1',
86.                  '10' : '1',
87.                  '20' : '2',
88.                  '30' : '3',
89.                  '60' : '4',
90.                  '120' : '5',
91.                  '300' : '1',
92.                  '1020' : '2',
93.                  '1021' : '3'}
94.
95.     keys = sort_images_keys(images)
96.
97.     fig, ax = plt.subplots()
98.     for key in keys:
99.         if normalize:
100.             spectrum = imgSpectrumNormalized(images[key])
101.         else:
102.             spectrum = imgSpectrum(images[key])
103.
104.             lines = ax.plot(eV, spectrum, label=key,
105.                            color=name2color[key[2:]],
106.                            linewidth=name2width[key[2:]])
107.
108.             ax.set(title='', ylabel=ylabel, xlabel=xlabel)
109.             ax.legend(loc='best')
110.
111.             if save:
112.                 plt.savefig(title+'.svg')
```

## E) PYTHON FUNCTIONS FOR PLOTTING DEVELOPMENT IN SPATIAL DRL/BB DISTRIBUTION

Functions for plotting the development in spatial DRL/BB distribution as described in Section 3.3.2 and seen in the C) figures of Figures 4.1 - 4.16 and Figures 4.17 - 4.20.

```

1. # -*- coding: utf-8 -*-
2.
3. import numpy as np
4. import matplotlib.pyplot as plt
5. import natsort
6. import os
7.
8. transisions = {'BB' : np.arange(29, 34),
9.               'D4' : np.arange(47, 52),
10.              'D3' : np.arange(58, 64),
11.              'D2' : np.arange(76, 82),
12.              'D1' : np.arange(92, 99),
13.              'D07': np.arange(115, 143),
14.              'DRL': np.arange(45, 200)}
15.
16.
17. def plot_transision(image, transision, title, cmap='gist_gray', vmin=None, vmax=None
18.                    , figsize=(19.20, 10.80), dpi=300):
19.     """
20.     Function that plots an image with the desired wavelength(s) from HSPL.
21.
22.     Parameters
23.     -----
24.     image : numpy.ndarray
25.         An array(y,x,wavelength) with HSPL images
26.     transision : numpy.ndarray
27.         Array of indeces of which wavelengths to display.
28.     title : string
29.         A string with a title for plot and figure.
30.     cmap : string
31.         matplotlib.pyplot (plt) color map to use.
32.     vmin : numeric or None
33.     vmax : numeric or None
34.     figsize : tuple(width, hight)
35.         See plt.figure documentation for figsize
36.     dpi : integer
37.         See plt.figure documentation for dpi
38.     """
39.
40.     plt.figure(title, figsize=figsize, dpi=dpi)
41.     plt.imshow(np.sum(image[:, :, transision], axis=2), cmap=cmap, vmin=vmin, vmax=v
42.               max)
43.     plt.axis('off')
44.     plt.colorbar()
45.     return
46.
47. def transision_plots(images, transision, title_addon, cmap='gist_gray', vmin=None, v
48.                     max=None,
49.                     figsize=(19.20, 10.80), dpi=300, save=False):
50.     """
51.     Function that displays all images provided by a dictionary.
52.     Made with Mehl20190131 and Mehl20190204 data in mind,
53.     or data of similar structure and naming scheme.
54.
55.     Parameters
56.     -----

```

## Appendices

```
56. images : dictionary
57.     A dictionary with the images (e.g. from one sample over time, as made by
58.     General.ReadFolders.read_crop_images_from_folders).
59. transision : string
60.     A string that names the transisions(wavelengths) to be displayed:
61.     'BB' 'D4' 'D3' 'D2' 'D1' 'D07' 'DRL'
62. title_addon : string
63.     A string with a suffix to add to the image title and saved file:
64.     'imagenam title_addon' (+.png)
65. cmap : string
66.     matplotlib.pyplot (plt) color map to use.
67. vmin : numeric or None
68. vmax : numeric or None
69.     matplotlib.pyplot (plt) vmin/vmax, or minimal/maximal intensity to display.
70. figsize : tuple(width, hight)
71.     See plt.figure documentation for figsize
72. dpi : integer
73.     See plt.figure documentation for dpi
74. save : bool
75.     True to save the displayed image as png-file.
76. """
77.
78. keys = sort_images_keys(images)
79.
80. for key in keys:
81.     plot_transision(images[key], transisions[transision], key+' '+title_addon,
82.                     cmap=cmap, vmin=vmin, vmax=vmax, figsize=figsize, dpi=dpi)
83.     if save:
84.         plt.savefig(key+' '+title_addon+'.png')
85. return
```





**Norges miljø- og biovitenskapelige universitet**  
Noregs miljø- og biovitenskapelige universitet  
Norwegian University of Life Sciences

Postboks 5003  
NO-1432 Ås  
Norway